JIRRS
Journal International Review of Research Studies

Received: 13/06/2026 - **Accepted:** 01/08/2026
Vol: 1.04
DOI: 10.66104/7x5etg23
Pages: 1-48

Slag Composition Control Indices in High-Temperature Metallurgy: A Critical Review of Viscosity, Conductivity, Corrosion, and Refractory Wear

Antonio Clareti Pereira, Ph.D.
Department of Graduate Program in Materials Engineering
Federal University of Ouro Preto (UFOP)
Ouro Preto, Minas Gerais, Brazil
E-mail: claretipereira@gmail.com
ORCID: https://orcid.org/0000-0001-8115-4279

Abstract

Metallurgical slag control is frequently reduced to one-dimensional composition indices, although industrial performance emerges from a coupled thermochemical state governed by melt structure, transport, phase stability, interfacial reactivity, refractory degradation, and process history. This critical review evaluates the physical meaning, calculation basis, calibration domain, and transferability of binary and extended basicity, optical basicity, structural descriptors, viscosity models, electrical-conductivity correlations, saturation and liquidus criteria, and data-driven approaches. Across the reviewed evidence, no single scalar index uniquely identifies the operating state of a multicomponent slag because temperature, redox state, amphoteric behavior, minor oxides, crystallization, solid fraction, and thermal history can alter property responses without changing the nominal index. Viscosity is the most extensively modeled property, whereas conductivity, corrosivity, and refractory wear are less consistently represented and are seldom incorporated into the same control logic. Cross-process comparison further indicates that indices calibrated for blast-furnace, mold-flux, gasification, copper-smelting, or refining slags should not be transferred without verifying compatibility in chemistry, thermal behavior, redox state, phase state, measurement method, and process history. The review therefore proposes a multi-property control framework that combines composition descriptors with thermodynamic phase state, structural metrics, property models, uncertainty bounds, and process-specific validation. This framework reframes slag control from fixed basicity targets toward dynamic state estimation and multi-objective operating windows supported by online sensing, CALPHAD-based calculations, structural models, and interpretable machine learning.

Keywords: slag basicity; optical basicity; slag viscosity; electrical conductivity; refractory corrosion; thermodynamic modeling

Highlights

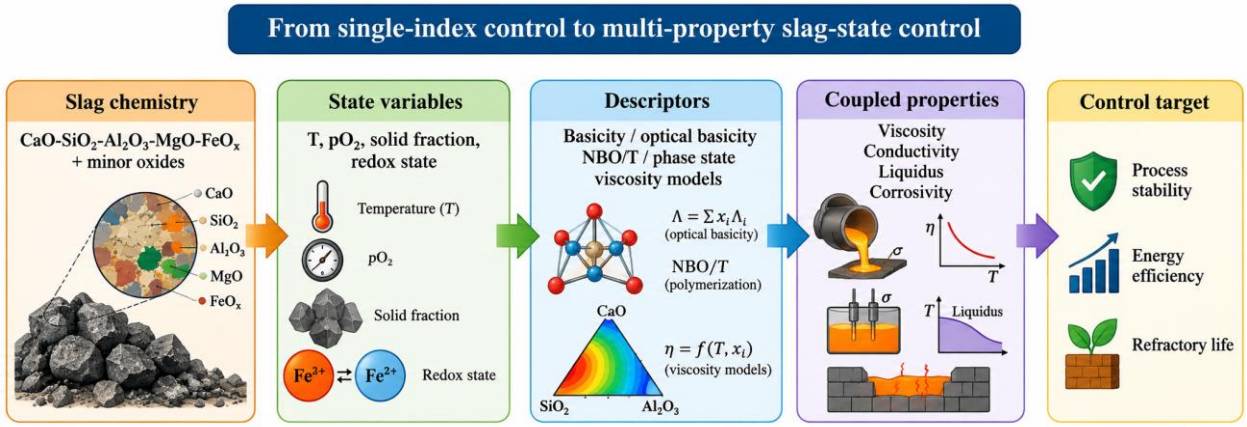
- No universal scalar slag index uniquely represents multicomponent high-temperature melts.
- Viscosity, conductivity, phase state, and refractory attack must be controlled as coupled properties.
- Index transferability is limited by chemistry, temperature, redox state, and crystallization.
- A multi-property framework links thermodynamics, structure, machine learning, and online sensing.

CC BY

JIRRS
Journal International Review of Research Studies

Received: 13/06/2026 - **Accepted:** 01/08/2026
Vol: 1.04
DOI: 10.66104/7x5etg23
Pages: 1-48

Graphical abstract



1. Introduction

Molten slags are functional process phases, not passive by-products. Their composition and physical state govern heat and mass transfer, metal-slag separation, reaction kinetics, refractory dissolution, electrical power distribution, inclusion absorption, foaming behavior, tapping, and overall process stability. Operators therefore rely on compact composition descriptors, especially basicity ratios, to convert multicomponent chemistry into rapid control targets. The operational advantage is clear: a scalar index is easy to calculate from routine chemical analysis and can be embedded in process practice. The scientific limitation is equally important: chemically distinct slags can share the same numerical index while exhibiting different structures, liquidus temperatures, viscosities, conductivities, crystallization tendencies, and interfacial reactivities (Kirschen et al., 2021; Muire et al., 2024; Pereira, 2026c; Zaaiman et al., 2024).

Recent experimental and modeling studies reinforce this non-uniqueness. Changes in MgO, BaO, MnO, TiO_2, Li_2O, FeO_x, or Al_2O_3 can reorganize silicate or aluminate networks in ways that are not captured by a single CaO/SiO_2 ratio, while the same bulk composition can move from a fully liquid state to a partially crystalline state as temperature changes (Chen et al., 2021; Liu & Zuo, 2025; Piao et al., 2023; Song et al., 2024; Xing et al., 2020; Yan et al., 2024). In Fe-bearing slags, redox state adds an extra degree of freedom because ionic and

CC BY

JIRRS
Journal International Review of Research Studies
Received: 13/06/2026 - **Accepted:** 01/08/2026
Vol: 1.04
DOI: 10.66104/7x5etg23
Pages: 1-48

electronic conduction may coexist; consequently, oxygen potential can alter transport behavior even when bulk oxide analysis is unchanged (Barati & Coley, 2006a, 2006b).

Figure 1 introduces the coupling among oxide roles, melt structure, transport properties, phase stability, and refractory response. Rather than treating basicity as a universal surrogate for slag state, Figure 1 frames composition control as a multi-property problem in which chemistry, temperature, redox state, and solid fraction jointly determine process-relevant behavior.

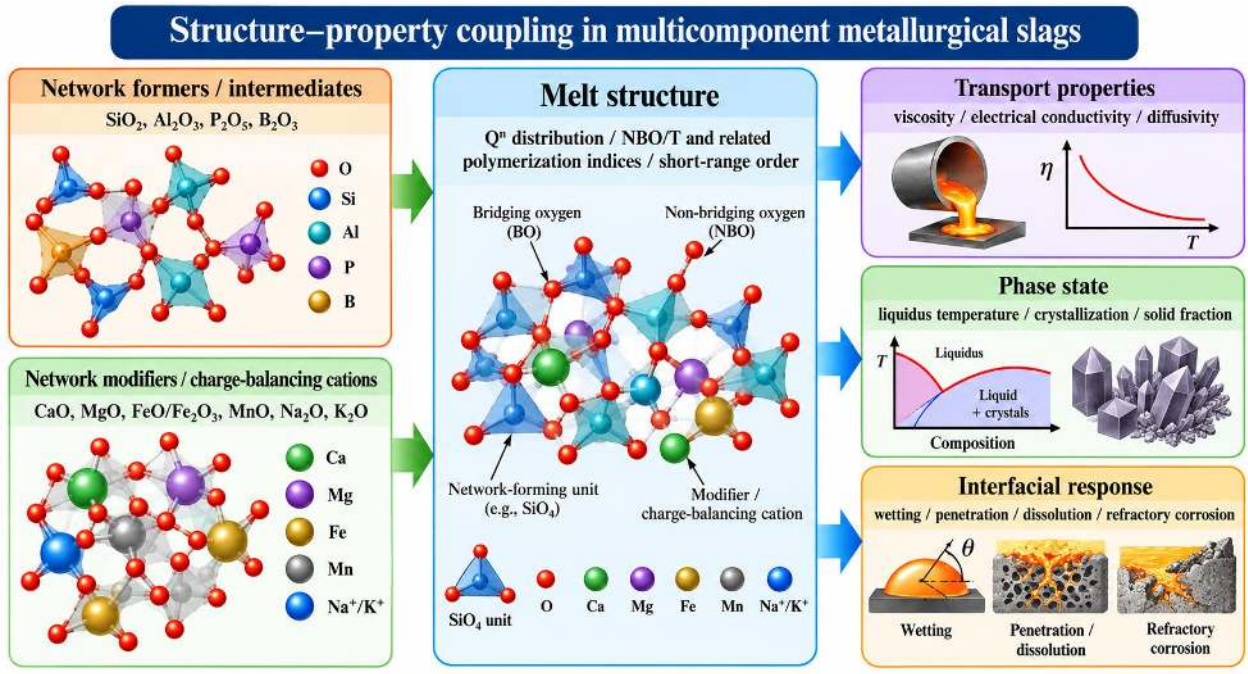


Figure 1. Structure-property coupling in multicomponent metallurgical slags.
Note. Developed by the author based on the structural and property relationships discussed by Muire et al. (2024), Sajid et al. (2020), and Zaaiman et al. (2024).

As Figure 1 shows, structural modification is an intermediate state variable between chemistry and macroscopic performance. Network formers and modifiers influence the distribution of oxygen species and short-range structural units, whereas temperature and phase stability determine whether those structural effects are expressed in a homogeneous liquid or in a multiphase suspension. Consequently, a robust control framework must distinguish composition descriptors, state descriptors, and directly predicted process properties.

CC BY

JIRRS
Journal International Review of Research Studies
Received: 13/06/2026 - **Accepted:** 01/08/2026
Vol: 1.04
DOI: 10.66104/7x5etg23
Pages: 1-48

Table 1 summarizes the conditional structural roles of the principal oxide groups. These categories are deliberately treated as context-dependent because several oxides, particularly Al_2O_3, Fe_2O_3, and TiO_2, can change structural function with composition, charge compensation, temperature, and redox environment.

Table 1. *Functional roles of major oxide groups in metallurgical slags and their implications for control indices.*

Oxide group	Representative oxides	Typical structural role	Control implication
Network formers	SiO_2, P_2O_5, B_2O_3	Increase network connectivity and polymerization	Often increase viscosity and lower ionic mobility, but response depends on modifiers and temperature
Network modifiers	CaO, MgO, FeO, MnO, Na_2O, K_2O, Li_2O	Generate non-bridging oxygen and depolymerize networks	Can reduce viscosity and alter conductivity; effects are nonlinear near saturation or crystallization
Amphoteric/intermediate oxides	Al_2O_3, Fe_2O_3, TiO_2, ZrO_2	Role changes with local charge compensation and composition	Simple basicity ratios may misclassify their contribution
Phase-forming components	MgO, CaO, Al_2O_3, Cr_2O_3, TiO_2	Control saturation, liquidus, and solid fraction	Property changes can be dominated by crystals rather than liquid structure

Note. Prepared by the author based on Chen et al. (2020, 2021), Sajid et al. (2020), Xing et al. (2020), and Muire et al. (2024).

Table 1 demonstrates why the expression "basic oxide" is an insufficient universal mechanistic label. A single composition change can alter network connectivity, charge balance, phase saturation, and interfacial chemical potential simultaneously. Property responses may therefore become non-monotonic, or even reverse direction, when the slag crosses a structural or phase boundary. On this basis, the present review critically assesses slag-composition control indices used for viscosity, electrical conductivity, liquidus and phase stability, corrosivity, and refractory wear, and it develops an integrated framework that separates rapid operational descriptors from physically interpretable state variables.

CC BY

JIRRS
Journal International Review of Research Studies

Received: 13/06/2026 - **Accepted:** 01/08/2026
Vol: 1.04
DOI: 10.66104/7x5etg23
Pages: 1-48

The evidence architecture of the review is explicit throughout the manuscript. Figure 1 and Table 1 define the structure-property basis and oxide roles; Table 2 and Figure 2 compare scalar indices and their non-uniqueness; Table 3 evaluates viscosity responses; Table 4 contrasts conductivity and refractory-control requirements; Table 5 addresses cross-process transferability; Table 6 compares modeling families; Figure 3 and Table 7 translate the synthesis into a validation framework; and Figure 4 extends that framework to closed-loop digital slag control.

2. Review methodology and literature scope

The literature search was conducted primarily in Google Scholar, with bibliographic verification against Crossref records and publisher journal pages when available. The final search update was completed on 3 October 2026. Thirteen topic-specific Boolean search families covered slag structure, binary and extended basicity, optical basicity, viscosity models, structure-viscosity relationships, electrical conductivity, slag-refractory interaction, erosion and transport, liquidus and crystallization, process-specific applications, limitations of existing indices, and thermodynamic, molecular, and machine-learning approaches. Representative search strings included: ("slag basicity" OR "extended basicity") AND (viscosity OR conductivity OR refractory); ("optical basicity" AND slag AND viscosity); (slag AND viscosity AND (Urbain OR Riboud OR Iida OR Mills)); ("electrical conductivity" AND slag AND (FeO OR redox OR "oxygen potential")); (slag AND refractory AND (corrosion OR erosion OR wetting OR infiltration)); (slag AND (liquidus OR crystallization OR "solid fraction") AND CALPHAD); and (slag AND viscosity AND ("machine learning" OR XGBoost OR SHAP OR hybrid)). We prioritized literature published from 2020 through 2026, while retaining earlier studies that established foundational index, conductivity, thermodynamic, or viscosity-model concepts.

Eligible sources were peer-reviewed journal articles and, when directly relevant to foundational models or industrial practice, peer-reviewed conference proceedings and authoritative technical chapters. Preprints, duplicate records, records lacking traceable bibliographic metadata, and studies without sufficient information to assess the relevant

CC BY

JIRRS
Journal International Review of Research Studies
Received: 13/06/2026 - **Accepted:** 01/08/2026
Vol: 1.04
DOI: 10.66104/7x5etg23
Pages: 1-48

composition/property relation were excluded. We applied no formal language restriction at discovery; final inclusion required sufficient English-language bibliographic and technical information for critical assessment. Duplicates were removed first by DOI and, when a DOI was unavailable, by normalized title, publication year, and first author. Backward citation searching from major reviews and foundational models, and forward citation searching for recent validation or extensions, were used to recover influential studies not captured by the initial queries. After revising and adding the requested seminal sources, the final corpus comprises 155 unique references.

The synthesis was organized by property and mechanism rather than by publication chronology. Evidence was considered transferable only when the chemical system, temperature range, redox condition, measurement method, phase state, and relevant process history were sufficiently defined for comparison. This restriction is essential because apparent disagreement among models often reflects different calibration domains or experimental protocols rather than genuine mechanistic contradiction. For each descriptor or model, the review asks four questions: which physical information is retained, which information is discarded, where the calibration domain lies, and which failure mode appears when the approach is transferred to another slag system. The study is a structured critical review, not a systematic review or meta-analysis; it aims to compare mechanisms, assess domain validity, and identify requirements for industrial transfer (Liu & Zuo, 2025; Yang et al., 2020).

3. Structure of molten slags and compositional descriptors

3.1. Network connectivity, amphoterism, and short-range order

Silicate-based slags are frequently interpreted through the balance between network-forming tetrahedral units and modifiers that create non-bridging oxygen. This language is useful because viscosity and ionic mobility are linked to the energy required for structural rearrangement. However, bulk oxide labels alone do not determine the structural state. First-principles calculations for $CaO–SiO_2–Al_2O_3$ systems show that changes in local coordination and bond topology accompany composition changes, while experimental and modeling work on $CaO–Al_2O_3$-based mold fluxes demonstrates that additives such as B_2O_3 and Li_2O can alter

CC BY

JIRRS
Journal International Review of Research Studies
Received: 13/06/2026 - **Accepted:** 01/08/2026
Vol: 1.04
DOI: 10.66104/7x5etg23
Pages: 1-48

both structure and viscosity beyond what simple binary basicity predicts (Chen et al., 2020, 2021; Sajid et al., 2020) (Bi et al., 2021; Haghdani et al., 2024; Ma et al., 2026; Song et al., 2024; Zhang et al., 2025).

Al_2O_3 is particularly important because it may behave as a network former when charge-compensating cations are available, yet its effect on viscosity can change when the available modifier inventory, CaO/Al_2O_3 ratio, or phase assemblage changes. TiO_2 shows similar system dependence: in some compositional windows it depolymerizes the network, while in others its influence is intertwined with crystallization and titanate phase formation. These effects explain why extended basicity expressions that simply place Al_2O_3 or TiO_2 in a denominator or numerator cannot be universal (Chen et al., 2020; Liu et al., 2022; Qi et al., 2026; Xiao et al., 2022; Zhao et al., 2024).

3.2. NBO/T and structural descriptors

The non-bridging oxygen per tetrahedron ratio (NBO/T) is more physically motivated than simple basicity because it reflects network connectivity. In the convention adopted here, NBO/T = N_NBO/N_T. For an ideal tetrahedral silicate/aluminosilicate network in which all oxygen belongs to tetrahedral units and oxygen triclusters/free oxygen are neglected, the equivalent bookkeeping expression is NBO/T = (2N_O/N_T) - 4. T denotes the number of tetrahedrally coordinated network-forming cations, with Si treated as tetrahedral and Al counted as tetrahedral only when charge compensation is explicitly available; other amphoteric or multivalent cations are included as network formers only when spectroscopic or atomistic evidence supports that allocation. Modifier charge is assigned first to charge compensation of tetrahedral Al before excess modifier charge is interpreted as generating non-bridging oxygen. Fe^{2+}/Fe^{3+} partitioning must be specified because Fe can change both charge balance and structural role.

These assumptions make NBO/T a domain-specific structural descriptor rather than a universal state variable. Transfer outside silicate-dominated, predominantly tetrahedral networks is not justified without independent structural validation, particularly for aluminate-dominant melts, fluoride-rich electroslag-remelting slags, highly Fe-rich redox-sensitive

CC BY

JIRRS
Journal International Review of Research Studies
Received: 13/06/2026 - **Accepted:** 01/08/2026
Vol: 1.04
DOI: 10.66104/7x5etg23
Pages: 1-48

systems, and strongly crystallizing multiphase slags. Raman, FTIR, NMR, XPS, molecular-dynamics, or first-principles evidence should therefore be used to validate the assumed cation allocation and coordination state whenever NBO/T is compared across composition families (Chen, Liu, et al., 2021; Lyu et al., 2025; Muire et al., 2024; Sajid et al., 2020; Zaaiman et al., 2024; Zhang, You, et al., 2026).

4. Basicity and optical basicity as control indices

4.1. Binary, ternary, and extended basicity

Binary basicity is defined here on a mass-fraction basis as $B_2 = w(CaO)/w(SiO_2)$, where w(i) is the mass fraction (or equivalently wt.% when the same units are used in numerator and denominator). A commonly used ternary extension is $B_3 = [w(CaO) + w(MgO)]/w(SiO_2)$. Extended basicity is represented generically as $B_ext = (\Sigma\ a_i\ w_i)/(\Sigma\ b_j\ w_j)$, where a_i and b_j are process-specific coefficients assigned to selected oxides. These coefficients, the included/excluded components, and the calibration range must always be reported; no single B_ext expression is treated here as universal. The main strength of these ratios is speed and interpretability. Their main weakness is mathematical compression: they map a high-dimensional chemical state onto a single number and therefore cannot distinguish two compositions with equal ratios but different absolute concentrations, redox states, or minor-oxide inventories (Bartzsch et al., 2023; Liu, Pang, et al., 2025; Sharpless et al., 2024; Yu et al., 2023).

This limitation becomes pronounced in high-Al_2O_3, high-TiO_2, Mn-rich, BaO-bearing, alkali-bearing, and CaO–Al_2O_3-based systems. Piao et al. (2023), Song et al. (2024), Xing et al. (2020), and Yan et al. (2024) each show that changing one modifier or amphoteric component can substantially alter structure and viscosity, even when conventional basicity changes little or remains conceptually ambiguous. Thus, basicity should be treated as a process-specific coordinate, not as a universal state variable (Liu, Wang, et al., 2025; Qin et al., 2022; Tian et al., 2025; Zhou et al., 2023).

CC BY

JIRRS
Journal International Review of Research Studies

Received: 13/06/2026 - **Accepted:** 01/08/2026
Vol: 1.04
DOI: 10.66104/7x5etg23
Pages: 1-48

4.2. Optical basicity

Duffy and Ingram (1976) developed optical basicity to represent the electron-donor power of oxide ions and provide a composition-weighted alternative to simple stoichiometric ratios. The calculation convention adopted in this review is $\Lambda = \Sigma X_i \Lambda_i$, where Λ_i is the assigned optical basicity of oxide i, and X_i is its equivalent oxygen fraction, X_i = n_iN_{O,i}/Σ(n_jN_{O,j}), with n_i the number of moles of oxide i and N_{O,i} the number of oxygen atoms contributed by its formula unit. Thus, oxide contributions are weighted by oxygen-equivalent fraction rather than by raw mass fraction. The adopted Λ_i values must be reported from the selected parameter set because alternative compilations can shift the numerical result. Optical basicity preserves oxide-specific acid-base weighting but still does not uniquely determine coordination, redox partitioning, phase fraction, or process history (Duffy & Ingram, 1976; Sharpless et al., 2024).

The distinction among principal scalar indices is summarized in Table 2. The comparison highlights that increasing mathematical sophistication does not automatically eliminate the state-information problem.

Table 2. *Comparison of scalar slag-composition indices used in high-temperature process control.*

Descriptor	Mathematical definition/convention	Composition basis	Intended use/domain	Key assumptions	Principal failure mode
Binary basicity, B_2	$B_2 = w(CaO)/w(SiO_2)$	Mass fraction (wt.% ratio)	Rapid local control in CaO-SiO_2-dominated slags	Same analytical basis; locally calibrated chemistry	Ignores other oxides, T, redox, and phase state
Ternary / extended basicity	$B_3 = [w(CaO)+w(MgO)]/w(SiO_2)$; $B_ext = (\Sigma a_i w_i)/(\Sigma b_j w_j)$	Usually mass fraction unless explicitly stated otherwise	Process-specific empirical extension	Coefficients and included oxides are calibration-specific	No universal coefficient set; amphoteric roles may reverse

CC BY

JIRRS
Journal International Review of Research Studies

Received: 13/06/2026 - **Accepted:** 01/08/2026
Vol: 1.04
DOI: 10.66104/7x5etg23
Pages: 1-48

Descriptor	Mathematical definition/convention	Composition basis	Intended use/domain	Key assumptions	Principal failure mode
Optical basicity, Λ	$\Lambda = \Sigma X_i \Lambda_i$; $X_i = n_i N_O,_i / \Sigma(n_j N_O,_j)$	Molar oxygen-equivalent fraction	Acid-base/electron-donor comparison across oxide mixtures	Requires selected Λ_i parameter set and oxide-speciation convention	Does not uniquely define structure, redox, or phase fraction
NBO/T	NBO/T = N_NBO/N_T; ideal tetrahedral bookkeeping: (2N_O/N_T) − 4	Atomic/molar structural count	Silicate-dominated tetrahedral networks	Explicit tetrahedral-former allocation, Al charge compensation, and Fe redox	Invalid if network topology, free O, coordination, or multiphase state violates assumptions
Liquidus margin, ΔT_L	$\Delta T_L = T_op - T_liquidus(x,pO_2)$	Temperature relative to modeled phase boundary	Thermal distance from first crystallization	Validated thermodynamic model/database for relevant components and redox	Equilibrium boundary may not represent transient plant state
Phase saturation ratio, S_p	S_p = a_p/a_p,sat (S_p = 1 at saturation)	Activity/composition-space proximity at fixed T and redox	MgO/spinel/magnetite or other phase saturation control	Defined reference phase and thermodynamic activity model	Sensitive to database/version, kinetics, and composition path

Note. Equations and conventions are defined explicitly for this review. Optical basicity follows Duffy and Ingram (1976) and the modern synthesis of Sharpless et al. (2024); structural and property limitations are synthesized from Muire et al. (2024) and Zaaiman et al. (2024). No extended-basicity coefficient set is assumed to be universal.

Table 2 indicates that scalar indices differ mainly in the physical information retained before dimensional reduction. Binary basicity preserves a major compositional ratio; optical basicity preserves oxide-specific acid-base weighting; NBO/T attempts to preserve network connectivity; and saturation indices preserve proximity to a phase boundary. None, however,

CC BY

JIRRS
Journal International Review of Research Studies

Received: 13/06/2026 - **Accepted:** 01/08/2026
Vol: 1.04
DOI: 10.66104/7x5etg23
Pages: 1-48

uniquely defines all properties required for industrial control. Figure 2 illustrates the practical consequence of this non-uniqueness.

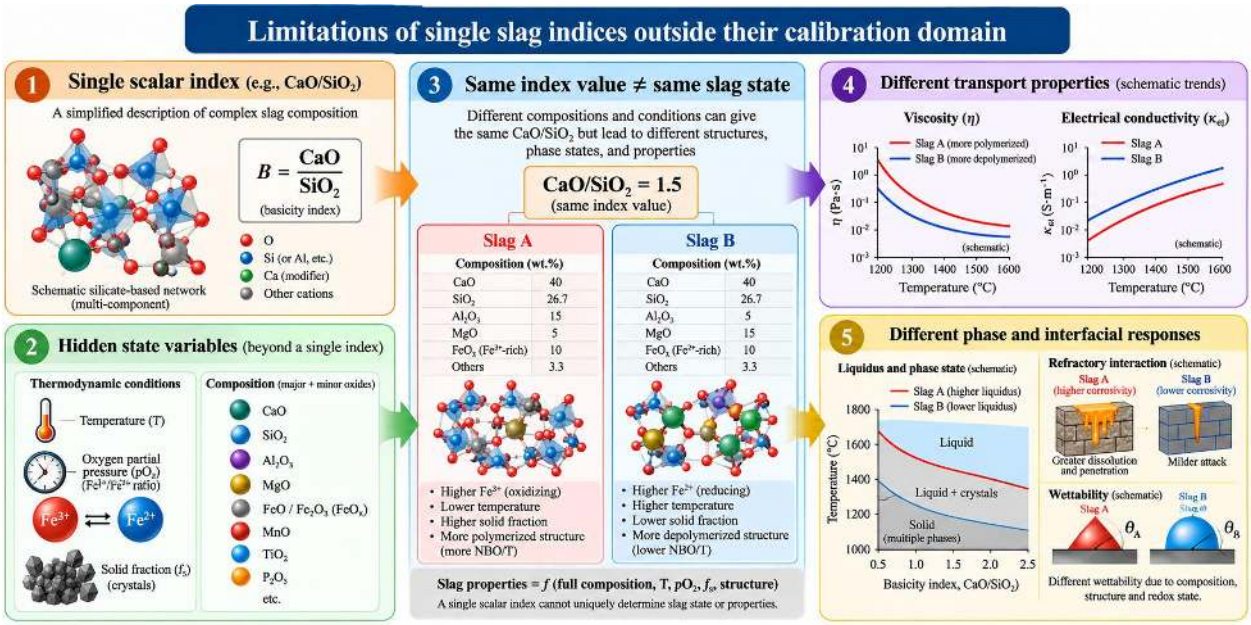


Figure 2. Illustrative non-uniqueness of scalar slag indices outside their calibration domain.
ILLUSTRATIVE CONCEPTUAL EXAMPLE — NOT A CALIBRATED DATASET
Note. Author-developed conceptual schematic. Curves and numerical relationships are illustrative examples only and are not fitted to, or calibrated against, a single experimental dataset.

Figure 2 emphasizes that identical basicity values can correspond to different temperatures, Fe^{2+}/Fe^{3+} ratios, solid fractions, and minor-oxide inventories. Accordingly, the operational value of a scalar index lies in local correlation within a constrained process window, and successful local calibration should not be interpreted as evidence of universality (Fan et al., 2021; Li, Xu, et al., 2023; Liu, Pang, et al., 2024; Nigam et al., 2026; Shishin et al., 2019; Xing et al., 2020).

5. Viscosity control indices and models

5.1. Empirical and thermodynamic viscosity models

Viscosity is the most extensively developed slag property in the control literature because it directly affects tapping, mixing, separation, infiltration, refractory mass transfer, and gas-slag interaction. Foundational semi-empirical formulations include the continuous-casting

CC BY

JIRRS
Journal International Review of Research Studies
Received: 13/06/2026 - **Accepted:** 01/08/2026
Vol: 1.04
DOI: 10.66104/7x5etg23
Pages: 1-48

model of Riboud et al. (1981), the Urbain model and its later synthesis (Urbain, 1987), the modified-basicity approach of Iida et al. (2000), and the optical-basicity-based treatment reviewed and compared by Mills and Sridhar (1999). These models reduce composition and temperature to a predicted viscosity through fitted structural or Arrhenius/Weymann-type parameters. Their practical value can be substantial within their calibration domains, but extrapolation remains hazardous near the liquidus, in high-Al_2O_3 systems, or when FeO_x, TiO_2, alkalis, fluorides, or other components move the melt outside the fitted structural regime (Iida et al., 2000; Kim & Min, 2021; Madej, 2025; Mills & Sridhar, 1999; Riboud et al., 1981; Urbain, 1987).

Thermodynamic viscosity approaches offer a stronger basis for transfer because they can couple composition to species or phase descriptions. Kim et al. (2021) modeled Fe-oxide-containing silicate melts under Fe-saturation conditions, whereas Pereira et al. (2023) evaluated viscosity behavior in CaO-SiO_2-Al_2O_3-MgO systems over a broad high-temperature range. These approaches improve physical consistency, but they remain dependent on thermodynamic-database quality, the viscosity parameterization, and the validity of the assumed phase state (Chen, Li, et al., 2021; Kim, Hudon, & Jung, 2021; Pereira et al., 2023; Shevchenko & Jak, 2020; Tan et al., 2023).

5.2. Component effects and structural interpretation

The common heuristic that SiO_2 increases viscosity whereas CaO and FeO decrease it is useful only within restricted, fully liquid domains. MgO and BaO can depolymerize the network, but they can also move the composition toward phase saturation. MnO can lower viscosity in some systems while simultaneously changing short-range order. Li_2O can strongly reduce viscosity in CaO-Al_2O_3-based mold fluxes, yet its effect depends on charge compensation, volatility, and crystallization behavior. These interactions are reported across mold-flux, blast-furnace, refining, and copper-related systems (Chen et al., 2021; Liu et al., 2024; Liu & Zuo, 2025; Madej, 2025; Piao et al., 2023; Song et al., 2024; Xing et al., 2020; Yan et al., 2024) (Jacob, 2024; Kong et al., 2021; Liu et al., 2026; Ren et al., 2024; Wang et al., 2023; Yuan & Zhu, 2022; Zhao, Qu, et al., 2021).

CC BY

JIRRS
Journal International Review of Research Studies
Received: 13/06/2026 - **Accepted:** 01/08/2026
Vol: 1.04
DOI: 10.66104/7x5etg23
Pages: 1-48

Table 3 summarizes the direction of commonly reported effects while explicitly separating structural and phase-state mechanisms.

Table 3

Qualitative effects of selected slag components on viscosity and the reasons simple index rules can fail.

Component change	Common fully liquid trend	Mechanistic interpretation	Major caveat
SiO_2 increase	Viscosity increases	Higher network connectivity	Effect depends on modifier availability and temperature
CaO increase	Viscosity decreases initially	Network depolymerization	Can increase solid fraction near saturation
FeO/FeO_x increase	Often decreases liquid viscosity	Strong modifier; redox-sensitive transport	Electronic conduction and phase equilibria also change
MgO increase	Often decreases then becomes non-monotonic	Modifier plus saturation control	Periclase/spinel formation may dominate
Al_2O_3 increase	System-dependent	Amphoteric; coordination and charge compensation vary	Cannot be assigned universally to numerator or denominator
Li_2O/alkali increase	Strong viscosity decrease in many fluxes	High field-effect modification and network disruption	Volatility, crystallization, and refractory compatibility constrain use
TiO_2 increase	System-dependent	Changes local structure and titanate phase stability	Response can reverse with chemistry and temperature

Note. Synthesized from Chen et al. (2021), Liu and Zuo (2025), Piao et al. (2023), Song et al. (2024), Xing et al. (2020), and Yan et al. (2024).

The critical implication of Table 3 is that viscosity is not a simple monotonic function of "basic" versus "acidic" oxide inventory. As the system approaches liquidus or crystallization, suspended solids and non-Newtonian behavior may control apparent viscosity more strongly than liquid-network depolymerization. Any viscosity index intended for process control should therefore include a phase-state criterion, or it should be explicitly restricted to a

CC BY

JIRRS
Journal International Review of Research Studies
Received: 13/06/2026 - **Accepted:** 01/08/2026
Vol: 1.04
DOI: 10.66104/7x5etg23
Pages: 1-48

fully liquid domain (Fan et al., 2026; Levchenko et al., 2025; Liu & Zuo, 2021; Mo et al., 2023; Shi, Tang, Chu, & Tian, 2026; Xie, Wang, et al., 2025; Zhang, He, et al., 2020).

5.4. Experimental comparability and rheological state

Viscosity datasets should not be pooled or used for machine-learning training without method metadata. At minimum, comparison requires the measurement geometry (e.g., rotating cylinder, concentric cylinder, oscillating cup, or other configuration), crucible and spindle materials, atmosphere and oxygen potential, temperature calibration and uncertainty, equilibration time, imposed shear rate or rotational speed, heating/cooling trajectory, and evidence that the measured state was fully liquid. The assumed rheological regime must also be stated: Newtonian viscosity in a homogeneous liquid is not equivalent to apparent viscosity measured after crystallization, precipitation, or particle suspension. Where solid fraction is non-negligible, the solid fraction, particle morphology, and thermal history should accompany the reported apparent viscosity. These controls are essential because crystallization can create non-monotonic viscosity-temperature behavior and because laboratory-to-laboratory differences can otherwise be misinterpreted as composition effects (Levchenko et al., 2025; Zaaiman et al., 2024).

5.3. Data-driven viscosity prediction

Machine learning has expanded the accessible composition space for viscosity prediction. Xuan et al. (2025) developed data-driven models for gasification-slag viscosity-temperature characteristics; Jia et al. (2026) combined machine learning with SHAP interpretation for steelmaking slags; Chen et al. (2026) incorporated domain knowledge in refining-slag prediction; and Singh et al. (2026) applied stacking regression. These approaches can outperform simple scalar correlations in multicomponent systems, but predictive accuracy alone does not establish mechanistic or cross-process transferability. Literature-derived datasets should therefore use source-grouped splitting where feasible, including leave-one-study-out validation and chemistry-domain holdout tests, rather than relying only on random train/test partitions that can place compositionally adjacent observations from the same publication in both sets. Training-set coverage, feature definition, temperature and phase-state

CC BY

JIRRS
Journal International Review of Research Studies
Received: 13/06/2026 - **Accepted:** 01/08/2026
Vol: 1.04
DOI: 10.66104/7x5etg23
Pages: 1-48

representation, data provenance, interpolation-versus-extrapolation status, external validation, and uncertainty quantification remain decisive (Chen et al., 2026; Jia et al., 2026; Saigo et al., 2022; Xuan et al., 2025).

6. Electrical conductivity and electrothermal slag control

Electrical conductivity is central to electroslag remelting, submerged-arc and electric smelting, electrically assisted refining, and emerging molten-oxide electrolysis concepts. In oxide melts, conductivity can contain both ionic and electronic contributions. Their relative importance depends on composition, temperature, oxygen potential, and the redox state of multivalent species. The classic CaO-SiO_2-FeO_x studies of Barati and Coley (2006a, 2006b) demonstrated that oxygen potential strongly affects the conductivity mechanism in Fe-bearing slags, directly limiting composition-only control (Barati & Coley, 2006a; Ju et al., 2025; Martin-Treceño et al., 2021; Stepanenko & Togobitska, 2026; Yang et al., 2023).

In many slag systems, viscosity and conductivity can move in opposite directions because depolymerization facilitates ionic motion while reducing viscous resistance; however, this relationship is not universal. Ionic species differ in mobility, FeO_x can introduce electronic pathways, and crystallization can simultaneously increase flow resistance and disrupt conductive networks. Viscosity should therefore not be used as an unqualified surrogate for electrical conductivity in electrothermal processes. Reviews by Muire et al. (2024) and Zaaiman et al. (2024) further show that conductivity datasets are substantially sparser than viscosity datasets, and that reported values remain sensitive to measurement method, atmosphere, and temperature control (Barati & Coley, 2006b; Judge & Azimi, 2020; Martin-Treceño et al., 2022; Stovpchenko et al., 2022; Yu et al., 2026).

Conductivity comparisons require the same discipline. Reports should distinguish total, ionic, and electronic conductivity and specify the measurement method, electrode geometry and spacing, electrode material, AC frequency or DC protocol, cell constant/calibration procedure, atmosphere, oxygen potential, temperature history, and whether polarization or interfacial effects were corrected. Conductivity should be reported consistently in S m^{-1} (or converted explicitly from other units). In Fe-bearing slags, total iron content cannot substitute

CC BY

JIRRS
Journal International Review of Research Studies
Received: 13/06/2026 - **Accepted:** 01/08/2026
Vol: 1.04
DOI: 10.66104/7x5etg23
Pages: 1-48

for Fe^{2+}/Fe^{3+} information because redox partitioning changes electronic transport independently of bulk FeO_x. Accordingly, viscosity may be discussed as a structurally related property, but it should never be used as an unqualified conductivity surrogate (Barati & Coley, 2006a, 2006b; Martin-Treceño et al., 2022).

Table 4 contrasts the information required for conductivity control with that required for refractory compatibility. The comparison shows why a basicity target adequate for fluidity may be insufficient for electrical or lining performance.

Table 4

Contrasting property descriptors for electrical conductivity and refractory degradation.

Control objective	Key state variables	Useful descriptors	Why basicity alone is insufficient
Electrical conductivity	T, Fe redox, alkali content, network connectivity, solid fraction	Conductivity model, optical basicity, FeO_x state, phase fraction	Does not represent charge-carrier concentration or electronic conduction
Flowability	T, liquid structure, crystals	Viscosity model, NBO/T, liquidus margin	Same basicity can produce different polymerization or solids
Refractory corrosion	Chemical potential gradients, saturation, wetting, flow	Saturation index, phase equilibria, viscosity, FeO_x/alkali activity	Attack depends on compatibility with specific refractory phases
Erosion/wear	Corrosion rate, hydrodynamics, particles, infiltration	Viscosity, density, velocity/shear, dissolution driving force	Wear couples chemical reaction with transport and mechanics

Note. Prepared by the author based on Barati and Coley (2006a, 2006b), Liu et al. (2025), Svantesson et al. (2021), and Zhang et al. (2026).

Table 4 shows that a composition change can improve one process target while degrading another. Lower viscosity may improve tapping or mass transfer, but it can also increase penetration into refractory pores or accelerate dissolution by reducing boundary-layer resistance. Conversely, increasing saturation with a refractory component may protect the

CC BY

JIRRS
Journal International Review of Research Studies
Received: 13/06/2026 - **Accepted:** 01/08/2026
Vol: 1.04
DOI: 10.66104/7x5etg23
Pages: 1-48

lining while narrowing the fully liquid operating window. A control index is therefore defensible only when the target property and the associated trade-offs are stated explicitly (Biswas et al., 2025; Kadylnykova et al., 2026; Martin-Treceño et al., 2020; Wiencke et al., 2020; Zaaiman et al., 2024).

7. Slag corrosivity, erosion, and refractory wear

7.1. Chemical compatibility and saturation

Refractory degradation results from coupled thermodynamic, kinetic, and mechanical processes. Dissolution is driven by chemical-potential differences between refractory phases and slag; infiltration depends on wetting, pore structure, capillary forces, and viscosity; reaction layers can either protect or destabilize the interface; and flow renews the boundary layer. High-FeO slags are particularly aggressive toward many steelmaking refractories, and dynamic testing confirms that wear cannot be inferred from composition alone (Svantesson et al., 2021) (Jing et al., 2026; Li, Liu, et al., 2023; Nazim et al., 2025; Song et al., 2020; Wei et al., 2025; Zhang, Zhu, et al., 2026).

For alumina-bearing refractories, slag basicity can alter dissolution pathways and spatial corrosion patterns. Peng et al. (2023) linked basicity to Turing-pattern corrosion behavior, while Zou et al. (2020) reported a quasi-volcanic corrosion phenomenon at an alumina refractory–slag–air interface. More recent work on iron-oxide-containing slags further emphasizes radical or reactive-species effects at alumina interfaces (Jing et al., 2026). These results show that interfacial geometry, atmosphere, and local chemistry can create mechanisms invisible to bulk basicity indices (Kaur et al., 2011; Liu et al., 2020; Pankka et al., 2026; Svantesson et al., 2021; Wu et al., 2022; Zhao, Zheng, et al., 2021).

7.2. MgO-based refractories and process-specific wear

MgO-based refractories are commonly protected by maintaining slag close to MgO saturation, but the optimal saturation condition depends on temperature, FeO_x content, spinel formation, carbon-containing refractory chemistry, and flow conditions. The comprehensive review by Liu et al. (2025) and the MgO–C-focused synthesis by Zhang et al. (2026) both

CC BY

JIRRS
Journal International Review of Research Studies
Received: 13/06/2026 - **Accepted:** 01/08/2026
Vol: 1.04
DOI: 10.66104/7x5etg23
Pages: 1-48

support a mechanism-based approach combining thermodynamic saturation with kinetic and microstructural evidence. Converter end-of-life investigations similarly show that cumulative service history produces spatially heterogeneous wear patterns that a single slag index cannot reconstruct (Pankka et al., 2026) (Lachmann & Scheller, 2025; Liu, Cheng, et al., 2025; Peng et al., 2023; Wang et al., 2025; Xie, Yin, et al., 2025; Zou et al., 2020).

Corrosion and erosion should therefore be separated conceptually. Corrosion is chemical and diffusional degradation, whereas erosion is material removal driven by flow, particles, bubbles, thermal cycling, or mechanically weakened reaction layers. Viscosity affects both processes, but not necessarily in the same direction: low viscosity can enhance convective mass transfer and infiltration, whereas high viscosity can increase hydrodynamic stresses in some particle-laden flows. A useful aggressiveness metric must therefore combine chemical driving force, transport intensity, and interfacial conditions (Lao et al., 2022; Moliné et al., 2026; Ribeiro et al., 2026; Wang et al., 2026; Yin et al., 2026).

7.3. Comparability of refractory-corrosion and wear evidence

Wear rates should be compared only after the test class is identified. Static cup tests primarily probe equilibrium approach, dissolution, wetting, and infiltration under limited boundary-layer renewal; rotating-finger, induction-furnace, flow-loop, or other dynamic tests introduce forced convection, erosion, and renewed interfacial transport; and industrial post-mortem observations integrate long service histories, thermal cycling, feed changes, local hydrodynamics, and repair practice. These evidence classes are complementary but not numerically interchangeable. Wetting angle, infiltration depth, boundary-layer renewal, velocity/shear, refractory porosity, and reaction-layer integrity should therefore accompany any attempt to compare corrosion or wear rates across studies. MgO saturation and spinel formation are treated as process-specific phase-state constraints, not universal lining-protection targets (Lao et al., 2022; Svantesson et al., 2021; Xie, Yin, et al., 2025).

CC BY

JIRRS
Journal International Review of Research Studies
Received: 13/06/2026 - **Accepted:** 01/08/2026
Vol: 1.04
DOI: 10.66104/7x5etg23
Pages: 1-48

8. Liquidus temperature, crystallization, and phase stability

Liquidus temperature and solid fraction are critical because a slag that is adequately fluid in the fully liquid state can become operationally unacceptable after modest cooling or composition drift. Crystallization can increase apparent viscosity, promote skull formation, cause plugging, alter electrical conductivity, and change heat-transfer behavior. Zhang et al. (2020) linked structure, viscosity, and crystallization in melts derived from blast-furnace slag, illustrating the need to treat these properties as coupled rather than independent. Yang et al. (2020) likewise modeled slag infiltration and heat transfer in continuous casting, where crystallization and viscosity jointly influence the flux-film function (Chebykin et al., 2025; Fan et al., 2014; Liao et al., 2023; Liu, Qin, et al., 2024; Sarkar & Li, 2021; Shishin et al., 2018; Yao et al., 2021).

A liquidus or saturation margin is often a more physically defensible operational descriptor than basicity because it measures proximity to a phase boundary. Two quantities should be distinguished. The thermal liquidus margin is defined here as $\Delta T_L = T_{op} - T_{liquidus}(x, pO_2)$, where positive values indicate operation above the predicted liquidus at composition x and the stated redox condition. By contrast, composition-space saturation at fixed temperature can be expressed for phase p as $S_p = a_p/a_{p,sat}$, with $S_p = 1$ at saturation; values below or above unity indicate undersaturation or supersaturation according to the adopted activity convention. These descriptors are not interchangeable. Their reliability depends on thermodynamic models and databases validated for the relevant multicomponent chemistry, and each reported result should identify the software, database, database version, included components, and redox constraints used in the calculation (Choi et al., 2021; He et al., 2021; Jung & Van Ende, 2020; Liao et al., 2023; Lyu et al., 2020).

Equilibrium phase boundaries should be interpreted as reference states rather than instantaneous furnace states. Residence time, thermal trajectory, reaction kinetics, mixing, transient feed changes, and prior crystallization/dissolution history can delay or redirect approach to equilibrium. Control systems should therefore report predicted liquidus temperature, saturation, or solid fraction together with model applicability, sensitivity,

CC BY

JIRRS
Journal International Review of Research Studies
Received: 13/06/2026 - **Accepted:** 01/08/2026
Vol: 1.04
DOI: 10.66104/7x5etg23
Pages: 1-48

uncertainty, and the time/history variables needed to judge whether equilibrium is a defensible approximation (Lin et al., 2025; Shen et al., 2024; Wang et al., 2022; Yeo et al., 2020).

9. Cross-process transferability of slag indices

The term "slag basicity" is used across blast furnaces, basic oxygen furnaces, electric arc furnaces, submerged-arc furnaces, copper and nickel smelting, ferroalloy production, electroslag remelting, and specialty refining, yet the dominant control objective differs among these operations. In blast furnaces, viscosity, desulfurization capacity, liquidus behavior, and hearth drainage may dominate. In steel refining, sulfur capacity, inclusion control, refractory compatibility, and foaming can be central. In copper smelting or converting, Fe/SiO_2 balance, magnetite saturation, matte-slag separation, and refractory interaction become decisive. Electrical processes add conductivity as a direct operating variable. Transferability must therefore be evaluated against both chemical domain and process function (Chen et al., 2015; Lai et al., 2026; Pereira, 2026c; Taskinen, 2011; Yan, Wang, et al., 2024; Zhao et al., 2013).

Table 5 summarizes these differences and identifies the main failure mode of applying a generic index outside its domain.

Table 5

Process-specific objectives and limitations of common slag-control indices.

Process	Primary slag-control objectives	Common descriptor family	Critical limitation
Blast furnace	Drainage, desulfurization, hot-metal/slag separation, liquidus control	Basicity + viscosity/liquidus models	High Al_2O_3, MgO reduction, and Ti-bearing slags alter structure and saturation
BOF/EAF/ladle	Refining capacity, foaming, inclusion control, refractory life	Basicity, FeO_x, MgO saturation, viscosity	Oxidation state and transient non-equilibrium conditions change rapidly
SAF/ferroalloys	Electrical resistance, tapping, metal–slag separation	Basicity + conductivity + viscosity	Conductivity and phase state can dominate over conventional basicity

CC BY

JIRRS
Journal International Review of Research Studies

Received: 13/06/2026 - **Accepted:** 01/08/2026
Vol: 1.04
DOI: 10.66104/7x5etg23
Pages: 1-48

Process	Primary slag-control objectives	Common descriptor family	Critical limitation
Copper/nickel smelting	Matte/metal separation, magnetite control, refractory compatibility	Fe/SiO_2, liquidus/saturation, viscosity	Redox and spinel/magnetite saturation must be included
Continuous casting flux	Lubrication, heat transfer, crystallization	Viscosity, break temperature, CaO/Al_2O_3 or CaO/SiO_2	Volatility, crystallization, and film state govern performance
ESR/electrothermal	Electrical heating, refining, interfacial control	Conductivity + viscosity + liquidus	Property coupling with temperature makes single-index control unstable

Note. Prepared by the author from the process-property relationships synthesized in Muire et al. (2024), Zaaiman et al. (2024), Madej (2025), and Yang et al. (2020).

The central message from Table 5 is that a "good slag" is not a universal composition but a process-dependent operating state that satisfies several constraints simultaneously. A transferable control framework should therefore define property windows rather than fixed index targets, and each window should be linked explicitly to the process function it protects (Gao et al., 2020; Lennartsson et al., 2019; Piao et al., 2023; Vítková et al., 2010; Yang et al., 2025).

Process-specific review evidence provides a complementary synthesis across metallothermic reduction, titanium-slag engineering, liquid-metal droplet recovery, and secondary-aluminum salt-slag treatment (Pereira, 2026a, 2026b, 2026c, 2026d, 2026e). These reviews are used here for cross-process synthesis only; mechanistic claims in the present review are supported preferentially by the primary experimental, thermodynamic, and modeling literature cited in the relevant sections.

10. Thermodynamic, structural, and data-driven modeling

10.1. CALPHAD and thermodynamic calculations

Thermodynamic software and CALPHAD-type databases provide a route from composition and temperature to phase equilibria, activities, saturation, and liquid fraction.

CC BY

JIRRS
Journal International Review of Research Studies
Received: 13/06/2026 - **Accepted:** 01/08/2026
Vol: 1.04
DOI: 10.66104/7x5etg23
Pages: 1-48

Quantitative predictions are reproducible only when the software, thermodynamic database, database version, modeled components, treatment of total Fe versus Fe^{2+}/Fe^{3+}, oxygen-potential/redox constraints, and imposed phases are reported. Their main advantage is mechanistic consistency across composition variables; their main limitations are database coverage and the equilibrium assumption. Industrial slags can be transient, compositionally heterogeneous, and kinetically constrained. Equilibrium calculations should therefore be interpreted as reference states and boundary estimates rather than automatic descriptions of the instantaneous process (Hidayat et al., 2017; Jung & Van Ende, 2020; Kim, Hudon, & Jung, 2021; Saito et al., 2025; Shevchenko & Jak, 2020).

For industrial interpretation, thermodynamic state should be augmented by process history: residence time, thermal trajectory, reaction and dissolution kinetics, mixing intensity, and transient feed changes determine how closely the actual slag approaches the predicted equilibrium state. A composition-temperature point can therefore map to different instantaneous phase fractions or interfacial conditions depending on its path. This history dependence is especially important near liquidus, saturation, and redox transitions.

10.2. Molecular and structural modeling

Molecular dynamics and first-principles calculations add information on coordination, bond networks, diffusion, and short-range structural species. Sajid et al. (2020) demonstrated how ab initio approaches can characterize $CaO\text{-}SiO_2\text{-}Al_2O_3$ slag structure. Such methods are especially useful as mechanistic support for explaining why empirical indices fail, but they do not constitute plant-scale validation. Their computational time/length scales, interatomic potentials or electronic-structure approximations, and restricted composition domains require careful mapping to experiments and industrial conditions (Haghdani et al., 2022; Ma et al., 2025; Song et al., 2023; Zhang, Min, et al., 2020).

10.3. Machine learning and interpretable hybrid models

Data-driven methods can interpolate complex nonlinear relationships without imposing a fixed analytical form. The strongest current direction is not purely black-box prediction but hybrid modeling that embeds thermodynamic or structural knowledge. Jia et al. (2026) used

CC BY

JIRRS
Journal International Review of Research Studies
Received: 13/06/2026 - **Accepted:** 01/08/2026
Vol: 1.04
DOI: 10.66104/7x5etg23
Pages: 1-48

SHAP analysis to interpret viscosity predictors; Chen et al. (2026) incorporated domain knowledge; Singh et al. (2026) used ensemble stacking; and Xuan et al. (2025) modeled viscosity-temperature behavior. SHAP feature importance should be interpreted as model-attribution information, not as proof of physical causation. Robust deployment requires preserved data provenance, source-grouped or leave-one-study-out validation, chemistry-domain holdout testing, explicit interpolation/extrapolation labeling, physically plausible trends, true external pilot/plant validation, model-domain boundaries, and uncertainty estimates such as calibrated prediction intervals. Out-of-distribution detection is required for online deployment so that states outside the validated domain trigger conservative fallback rather than confident extrapolation (Chen et al., 2026; Huang et al., 2020; Jia et al., 2026; Li et al., 2022; Shi, Tang, Chu, & Tian, 2026; Yan, Shen, et al., 2024).

Table 6 compares the principal modeling families and their intended roles in process control.

Table 6

Comparison of modeling approaches for slag-state prediction and control.

Approach	Primary output	Strength	Deployment limitation
Empirical scalar index	Single descriptor	Fast and transparent	Low dimensionality; system-specific calibration
Empirical viscosity equation	Viscosity vs composition and T	Low computational cost	Extrapolation risk and phase-state sensitivity
CALPHAD/thermodynamics	Phases, activities, liquidus, saturation	Physically consistent equilibrium framework	Database quality; equilibrium may not reflect transients
Molecular/first-principles	Structure, coordination, diffusion	Mechanistic interpretation	High computational cost and limited system size/time
Machine learning	Nonlinear property prediction	Handles high-dimensional composition spaces	Requires representative training data and uncertainty control

CC BY

JIRRS
Journal International Review of Research Studies

Received: 13/06/2026 - **Accepted:** 01/08/2026
Vol: 1.04
DOI: 10.66104/7x5etg23
Pages: 1-48

Approach	Primary output	Strength	Deployment limitation
Hybrid physics + ML	Property/state estimation with physical constraints	Promising combination of physical constraints, transferability, and interpretability	Not a universal solution; integration complexity, domain monitoring, and external plant validation remain mandatory

Note. Synthesized from Sajid et al. (2020), Pereira et al. (2023), Jia et al. (2026), Chen et al. (2026), Singh et al. (2026), and Xuan et al. (2025).

Table 6 indicates that these modeling families should be treated as a hierarchy of complementary tools rather than as competing alternatives. Scalar indices remain useful as operator-facing summaries; thermodynamic models define phase-state constraints; atomistic methods help explain structural mechanisms; and machine-learning models can capture high-dimensional nonlinear relationships. The strongest control architecture is consequently hybrid: physical models constrain the feasible state space, data-driven models refine property estimates within that space, and uncertainty metrics identify when the process is approaching the edge of the validated domain (Jung & Van Ende, 2020; Peng et al., 2020; Shevchenko & Jak, 2020; Shishin et al., 2021).

11. Critical limitations and an integrated multi-property framework

Six recurring failure modes emerge from the reviewed literature. First, compositional non-uniqueness allows chemically different slags to share the same index. Second, temperature dependence permits a fixed composition to cross liquidus or structural transitions without any change in the index. Third, redox dependence is lost when total iron is represented without the Fe^{2+}/Fe^{3+} state. Fourth, multicomponent interactions create amphoteric and non-additive effects. Fifth, process transfer assumes that the property controlling one unit operation also controls another. Sixth, time and process history are omitted even though residence time, thermal trajectory, reaction kinetics, mixing, and transient feed changes can make the instantaneous state depart from equilibrium. These are not minor corrections to an otherwise universal descriptor; taken together, they explain why no universal scalar slag index is physically sufficient (Nagata & Sasabe, 2020; Pereira, 2026c).

CC BY

JIRRS
Journal International Review of Research Studies

Received: 13/06/2026 - **Accepted:** 01/08/2026
Vol: 1.04
DOI: 10.66104/7x5etg23
Pages: 1-48

A practical alternative is the six-layer framework shown in Figure 3. The framework preserves the operational simplicity of index-based control while preventing an index from being mistaken for the full state description.

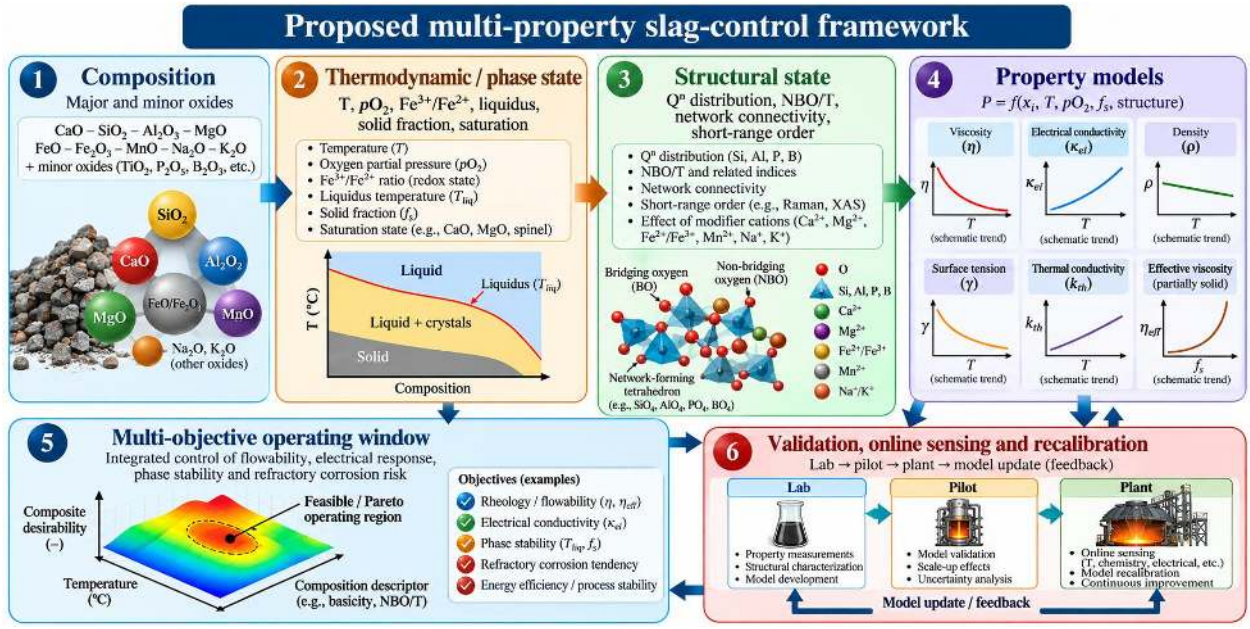


Figure 3. Illustrative author-developed multi-property framework for high-temperature slag control.

ILLUSTRATIVE AUTHOR-DEVELOPED FRAMEWORK — NOT AN INDUSTRIAL STANDARD

Note. Author-developed conceptual framework based on the critical synthesis in this review. The optimization surface is illustrative and is not generated from a calibrated dataset; the framework is not presented as a validated industrial standard.

As shown in Figure 3, chemistry remains the first layer because it is measurable and actionable. It is then followed by thermodynamic state, structural state, property models, and uncertainty before an operating decision is made. The decision target is a process-specific multi-objective or Pareto operating window rather than a universal composite score: sufficient flowability, suitable electrical response where relevant, acceptable liquidus margin, chemical compatibility with the refractory system, and any process-specific quality or separation constraint. Priorities and constraints must be defined separately for each process. The final validation layer explicitly tests whether a model calibrated in the laboratory remains valid at pilot and industrial scales and whether it remains inside the validated domain after chemistry or operating-practice changes.

CC BY

JIRRS
Journal International Review of Research Studies
Received: 13/06/2026 - **Accepted:** 01/08/2026
Vol: 1.04
DOI: 10.66104/7x5etg23
Pages: 1-48

Table 7 converts the conceptual framework into a validation checklist for index deployment.

Table 7

Minimum validation requirements before transferring a slag index or model to a new process domain.

Validation question	Required evidence	Failure if omitted
Is chemistry within calibration domain?	Ranges for all major/minor oxides	Hidden extrapolation and false confidence
Is temperature/phase state represented?	Liquidus margin, solid fraction, T range	Abrupt viscosity or conductivity errors near crystallization
Is redox state relevant?	Fe^{2+}/Fe^{3+} or oxygen-potential information	Incorrect conductivity, activity, or corrosion prediction
Is refractory compatibility included?	Saturation and interfacial reaction assessment	Good fluidity but unacceptable wear
Are measurements method-consistent?	Documented viscosity/conductivity protocol	Apparent model error caused by incompatible datasets
Has uncertainty been quantified?	Prediction intervals or sensitivity analysis	No criterion for safe operation near limits
Has the model been externally validated?	Independent study, pilot, or plant data outside the model-training source groups	Overfitting or source leakage can masquerade as transferability
Are model and database versions controlled?	Software/model identifier, thermodynamic database name and version, parameter-set version, and change log	Silent version drift prevents reproducibility and can shift phase/property predictions
Is measurement uncertainty represented?	Instrument calibration, uncertainty bounds, method metadata, and propagated property uncertainty	False precision and inconsistent weighting of heterogeneous literature data
Is process history compatible?	Residence time, thermal trajectory, feed-change history, mixing/reaction time, and prior crystallization/dissolution state	Same composition and temperature may correspond to a different instantaneous state

Note. Prepared by the author based on the recurring limitations identified across the studies reviewed here.

The checklist in Table 7 makes transferability falsifiable. Instead of asking whether an index simply "works," the more rigorous question is whether the target operating state remains

CC BY

JIRRS
Journal International Review of Research Studies
Received: 13/06/2026 - **Accepted:** 01/08/2026
Vol: 1.04
DOI: 10.66104/7x5etg23
Pages: 1-48

inside a chemically, thermally, redox-, phase-, measurement-, and process-compatible validation domain. Failure to document these boundaries converts a local empirical correlation into an unsupported universal claim.

12. Future directions: online sensing and digital slag metallurgy

Future slag control will likely move from periodic chemistry correction toward continuous state estimation. The necessary building blocks already exist separately: faster compositional analysis, thermal imaging, electrical measurements, thermodynamic calculations, interpretable machine learning, and process historians. The central research challenge is to fuse these data streams into a control architecture that distinguishes measurement noise from genuine movement toward phase, viscosity, conductivity, or refractory-risk boundaries (Klaffenbach et al., 2021; Meratian et al., 2021; Singh et al., 2026; Weiss et al., 2026; Zhang et al., 2021).

Figure 4 shows a prospective closed-loop architecture in which validated sensor data feed a state estimator, hybrid thermodynamic-structural-machine-learning models predict the multi-property slag state, and a constrained optimizer proposes feasible actions such as flux addition, feed adjustment, or power modification. The architecture is author-developed and conceptual; it is not presented as an already implemented or validated industrial control system.

CC BY

JIRRS
Journal International Review of Research Studies

Received: 13/06/2026 - **Accepted:** 01/08/2026
Vol: 1.04
DOI: 10.66104/7x5etg23
Pages: 1-48

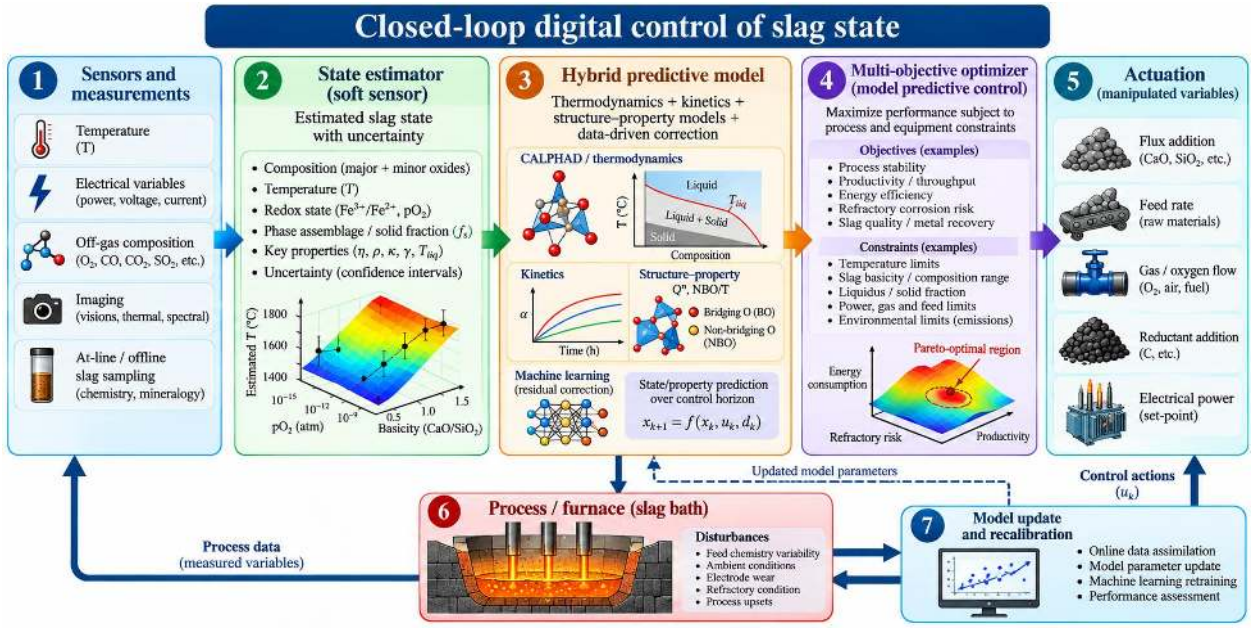


Figure 4. Prospective author-developed digital architecture for future slag-state control.
PROSPECTIVE AUTHOR-DEVELOPED ARCHITECTURE — REQUIRES INDUSTRIAL VALIDATION

Note. Prospective author-developed conceptual architecture based on current thermodynamic, sensing, and machine-learning approaches. It is not an implemented industrial standard and requires process-specific validation.

The central requirement in Figure 4 is feedback validation. Sensor health and calibration should be checked before state estimation; sensor failure or disagreement should trigger fault handling rather than automatic optimization. Model predictions should carry uncertainty and out-of-distribution flags. The optimizer must respect actuator limits, feasible rates of flux/feed/power change, and control latency. When uncertainty exceeds an approved threshold or the state is outside the validated domain, the system should revert to a safe fallback or manual-control mode with explicit operator oversight. A digital model should not remain static after commissioning; it should detect domain drift and trigger recalibration when chemistry, feed conditions, refractory practice, sensor configuration, or operating strategy moves outside the training or calibration envelope.

A second research priority is the development of synchronized multi-property datasets in which viscosity, total/ionic/electronic conductivity where relevant, liquidus or solid fraction, and refractory interaction are measured or modeled for the same compositions, temperatures,

CC BY

JIRRS
Journal International Review of Research Studies
Received: 13/06/2026 - **Accepted:** 01/08/2026
Vol: 1.04
DOI: 10.66104/7x5etg23
Pages: 1-48

redox conditions, and thermal histories. Each record should preserve measurement-method metadata, calibration information, uncertainty, atmosphere, geometry/electrode configuration where applicable, and provenance at the study/laboratory level. Current datasets are fragmented by property and laboratory method. Without synchronized multi-property datasets, optimization remains sequential, and control actions can improve one response while degrading another (Gao et al., 2017; Lee et al., 2025; Muire et al., 2024; Xia et al., 2024; Zheng et al., 2023).

13. Conclusion

Slag composition control cannot be reduced reliably to a universal scalar index. Binary and extended basicity remain useful operational coordinates, while optical basicity and NBO/T provide progressively richer chemical or structural interpretation; however, none uniquely defines the thermochemical state of a multicomponent slag. Viscosity, electrical conductivity, liquidus and solid fraction, corrosion, and refractory wear respond to overlapping but non-identical combinations of composition, temperature, redox state, structure, phase stability, measurement context, and process history. The fundamental limitation of scalar indices is therefore information loss during dimensional reduction, particularly near phase, redox, or structural boundaries.

A more robust strategy is to retain simple indices as front-line descriptors while embedding them in a multi-property framework that includes thermodynamic phase state, structural metrics, calibrated viscosity and conductivity models, refractory-compatibility criteria, uncertainty bounds, and process-specific validation. CALPHAD calculations, atomistic descriptions, online sensing, and interpretable machine learning are most valuable when they are combined rather than substituted for one another. Future progress therefore depends less on proposing additional universal ratios and more on defining validated, uncertainty-aware, process-specific multi-objective operating windows that can be updated as chemistry, redox state, thermal conditions, sensor validity, and process history evolve.

CC BY

JIRRS
Journal International Review of Research Studies

Received: 13/06/2026 - **Accepted:** 01/08/2026
Vol: 1.04
DOI: 10.66104/7x5etg23
Pages: 1-48

Declarations

Funding

This review received no specific external funding.

Conflict of interest

The author declares no conflict of interest.

Data availability

No new experimental datasets were generated. All quantitative and bibliographic information discussed in the review is traceable to the cited literature.

Author contributions

The author performed conceptualization, critical analysis, literature synthesis, visualization, and manuscript preparation.

References

1. Barati, M., & Coley, K. S. (2006a). Electrical and electronic conductivity of CaO-SiO_2-FeO_x slags at various oxygen potentials: Part I. Experimental results. Metallurgical and Materials Transactions B, 37(1), 41–49.

2. Barati, M., & Coley, K. S. (2006b). Electrical and electronic conductivity of CaO-SiO_2-FeO_x slags at various oxygen potentials: Part II. Mechanism and a model of electronic conduction. Metallurgical and Materials Transactions B, 37(1), 51–60.

3. Bartzsch, G., Christian, R., Mohanty, S. R., Shukla, A. K., & Volkova, O. (2023). Effect of Al_2O_3 and TiO_2 on viscosity, surface tension and density of blast furnace slag at CaO/SiO_2 = 1.13. Steel Research International, 94, 2200798.

4. Bi, Z., Li, K., Jiang, C., Zhang, J., Ma, S., Sun, M., Wang, Z., & Li, H. (2021). Effects of B_2O_3 on the structure and properties of blast furnace slag by molecular dynamics simulation. Journal of Non-Crystalline Solids, 551, 120412.

CC BY

JIRRS
Journal International Review of Research Studies

Received: 13/06/2026 - **Accepted:** 01/08/2026
Vol: 1.04
DOI: 10.66104/7x5etg23
Pages: 1-48

5. Biswas, J., Hazaveh, P. K., & Coley, K. S. (2025). Slag electrical conductivity and its effect on mass transport and interfacial reaction kinetics. Steel Research International, 96(4), 2300701.

6. Chebykin, D., Heller, H.-P., Schulz, K., Endo, R., & Volkova, O. (2025). Viscosity, density, surface tension, and crystallization behavior of commercial mold fluxes. Steel Research International, 96, 2400103.

7. Chen, J., Feng, Y., Zhang, Y., Luan, J., Lu, X., Yu, Z., & Chou, K. (2026). Viscosity prediction of refining slag based on machine learning with domain knowledge. International Journal of Minerals, Metallurgy and Materials, 33(2), 555–566.

8. Chen, J.-B., Li, J.-G., Chu, R., & Sun, Y.-Q. (2021). Thermodynamic activity of FeO in CaO–SiO_2–MnO–FeO–MgO molten slags. Ironmaking & Steelmaking, 48(10), 1239–1246.

9. Chen, L., Guo, M., Shi, H., Scheunis, L., Jones, P. T., Blanpain, B., & Malfliet, A. (2015). The influence of ZnO in fayalite slag on the degradation of magnesia-chromite refractories during secondary Cu smelting. Journal of the European Ceramic Society, 35(9), 2641–2650.

10. Chen, L., Liu, K., Han, P., Yang, B., & Feng, L. (2020). Calculation and analysis of the structure and viscosity of B_2O_3-regulated CaO-Al_2O_3-based mold fluxes. Journal of Chemistry, 2020, 8844392.

11. Chen, L., Liu, K., Han, P., Yang, B., & Feng, L. (2021). Effects of Li_2O on structure and viscosity of CaO-Al_2O_3-based mold fluxes. Journal of Chemistry, 2021, 6674453.

12. Choi, J. S., Park, T. J., & Min, D. J. (2021). Structure–property relationship amphoteric oxide systems via phase stability and ionic structural analysis. Journal of the American Ceramic Society, 104(1), 140–156.

13. Duffy, J. A., & Ingram, M. D. (1976). An interpretation of glass chemistry in terms of the optical basicity concept. Journal of Non-Crystalline Solids, 21(3), 373–410. https://doi.org/10.1016/0022-3093(76)90027-2

CC BY

JIRRS
Journal International Review of Research Studies

Received: 13/06/2026 - **Accepted:** 01/08/2026
Vol: 1.04
DOI: 10.66104/7x5etg23
Pages: 1-48

14. Fan, C., Huang, H., Wang, H., Lu, W., Meng, Q., & Long, H. (2026). Comparative study of MgO and MnO in regulating viscosity, meltability and structure of blast furnace slag with 20% Al_2O_3. Ceramics International, 52(17), 32671–32678.

15. Fan, L., Liu, C., Qi, J., & Jiang, M. (2021). Effect of La_2O_3 on the viscosity, crystallization, and structure of calcium-silicate-based mold flux for continuous casting La-bearing FeCrAl alloy. ISIJ International, 61(8), 2193–2199.

16. Fan, Y., Shibata, E., Iizuka, A., & Nakamura, T. (2014). Crystallization behaviors of copper smelter slag studied using time-temperature-transformation diagram. Materials Transactions, 55, 958–963.

17. Gao, X., Chen, Z., Shi, J., Taskinen, P., & Jokilaakso, A. (2020). Effect of cooling rate and slag modification on the copper matte in smelting slag. Mining, Metallurgy & Exploration, 37, 1593–1601.

18. Gao, Y., Yang, C., Zhang, C., Qin, Q., & Chen, G. Z. (2017). Magnesia-stabilised zirconia solid electrolyte assisted electrochemical investigation of iron ions in a SiO_2–CaO–MgO–Al_2O_3 molten slag at 1723 K. Physical Chemistry Chemical Physics, 19, 15876–15890.

19. Haghdani, S., Tangstad, M., & Einarsrud, K. E. (2022). A Raman-structure model for the viscosity of SiO_2-CaO-Al_2O_3 system. Metallurgical and Materials Transactions B, 53, 1733–1746.

20. Haghdani, S., Tangstad, M., & Einarsrud, K. E. (2024). Studying the structure and viscosity of MnO-SiO_2-CaO-Al_2O_3-MgO slag system. Materials, 17(15), 3789.

21. He, C., Ilyushechkin, A., Bai, J., Hla, S. S., Kong, L.-X., & Li, W. (2021). Viscosity and crystallisation behaviour of coal ash slag from the primary phase of anorthite. Fuel Processing Technology, 213, 106680.

22. Hidayat, T., Shishin, D., Decterov, S. A., & Jak, E. (2017). Critical assessment and thermodynamic modeling of the Cu–Fe–O–Si system. CALPHAD: Computer Coupling of Phase Diagrams and Thermochemistry, 58, 101–114.

CC BY

JIRRS
Journal International Review of Research Studies

Received: 13/06/2026 - **Accepted:** 01/08/2026
Vol: 1.04
DOI: 10.66104/7x5etg23
Pages: 1-48

23. Huang, A., Huo, Y., Yang, J., Gu, H., & Li, G. (2020). Computational modeling and prediction on viscosity of slags by big data mining. Minerals, 10(3), 257.

24. Iida, T., Sakai, H., Kita, Y., & Shigeno, K. (2000). An equation for accurate prediction of the viscosities of blast furnace type slags from chemical composition. ISIJ International, 40(Suppl.), S110–S114. https://doi.org/10.2355/isijinternational.40.Suppl_S110

25. Jacob, L. (2024). Ladle furnace slag: Synthesis, properties, and applications. ChemBioEng Reviews, 11(1), 60–78.

26. Jia, G., Zhao, R., & Yan, W. (2026). Interpretable viscosity prediction of steelmaking slag integrating machine learning with SHAP explanation. Journal of Non-Crystalline Solids, 676, 123955.

27. Jing, X., Li, S., Huang, A., Jiang, G., Zeng, F., Xie, Q., Zhao, Z., & Gu, H. (2026). Iron oxide containing slag corrosion mechanism on the alumina refractory ceramic: Role of aluminum ion radicals. Ceramics International, 52(18), 33516–33528.

28. Ju, J., He, K., Qiu, G., & Zhou, Y. (2025). Effect of CaO/Al_2O_3 on electrical conductivity, viscosity and structure of electroslag remelting-type TiO_2-bearing slag. Ironmaking & Steelmaking, 52(1), 98–106.

29. Judge, W. D., & Azimi, G. (2020). Thermodynamic and kinetic modelling of molten oxide electrolysis cells. In TMS 2020 Supplemental Proceedings (pp. 1923–1932). Springer.

30. Jung, I.-H., & Van Ende, M.-A. (2020). Computational thermodynamic calculations: FactSage from CALPHAD thermodynamic database to virtual process simulation. Metallurgical and Materials Transactions B, 51, 1851–1874.

31. Kadylnykova, A., Wu, M., & Kharicha, A. (2026). Fluoride partitioning and Al-O-F coordination dynamics control ionic conductivity in CaF_2-Al_2O_3 electroslag remelting slags. Journal of Solid State Chemistry, 361, 126127.

CC BY

JIRRS
Journal International Review of Research Studies

Received: 13/06/2026 - **Accepted:** 01/08/2026
Vol: 1.04
DOI: 10.66104/7x5etg23
Pages: 1-48

32. Kaur, R. R., Swinbourne, D. R., Wadsley, M. W., & Nexhip, C. (2011). Comparison of ferrous calcium silicate slag and calcium ferrite slag interactions with magnesia-chrome refractories. Metallurgical and Materials Transactions B, 42, 451–459.

33. Kim, W. Y., Hudon, P., & Jung, I. H. (2021). Modeling the viscosity of silicate melts containing Fe oxide: Fe saturation condition. Calphad, 72, 102242.

34. Kim, W.-Y., Hudon, P., & Jung, I.-H. (2021). Modeling the viscosity of silicate melts containing Fe oxide: FeO/Fe_2O_3 containing system. Calphad, 72, 102244.

35. Kim, Y., & Min, D.-J. (2021). Viscosity and structural investigation of high-concentration Al_2O_3 and MgO slag system for FeO reduction in electric arc furnace processing. Metals, 11(8), 1169.

36. Kirschen, M., Hay, T., & Echterhof, T. (2021). Process improvements for direct reduced iron melting in the electric arc furnace with emphasis on slag operation. Processes, 9, 402.

37. Klaffenbach, E., Mostaghel, S., Guo, M., & Blanpain, B. (2021). Thermodynamic analysis of copper smelting, considering the impact of minor elements behavior on slag application options and Cu-recovery. Journal of Sustainable Metallurgy, 7, 664–683.

38. Kong, L., Bai, J., & Li, W. (2021). Viscosity-temperature property of coal ash slag at the condition of entrained flow gasification: A review. Fuel Processing Technology, 215, 106751.

39. Lachmann, S., & Scheller, P. R. (2025). Effect of chemistry and external electric potential on interfacial tension between steel and slag. Steel Research International, 96(8), 2401028.

40. Lai, C., Jing, B., Tan, J., & Li, Q. (2026). Investigation of iron droplets assembling in molten slag. Colloids and Surfaces A: Physicochemical and Engineering Aspects, 735, 139463.

CC BY

JIRRS
Journal International Review of Research Studies

Received: 13/06/2026 - **Accepted:** 01/08/2026
Vol: 1.04
DOI: 10.66104/7x5etg23
Pages: 1-48

41. Lao, Y., Li, G., Gao, Y., & Yuan, C. (2022). Wetting and corrosion behavior of MgO substrates by CaO–Al_2O_3–SiO_2–(MgO) molten slags. Ceramics International, 48(10), 14799–14812.

42. Lee, K.-D., Seo, W.-G., Gupta, A., & Choi, S.-H. (2025). Effect of composition and temperature on the viscosity and electrical conductivity of ferronickel slags. Metals, 15(11), 1237.

43. Lennartsson, A., Engström, F., Björkman, B., & Samuelsson, C. (2019). Understanding the bottom buildup in an electric copper smelting furnace by thermodynamic calculations. Canadian Metallurgical Quarterly, 58(1), 89–95.

44. Levchenko, M., Tinkova, N., Yehorov, A., Endo, R., & Volkova, O. (2025). Factors influencing slag viscosity measurements using the Concentric Cylinder Measuring System at high temperatures. Journal of Non-Crystalline Solids, 666, 123647.

45. Li, C., Xi, W., Wang, C., Lin, X., Xu, D., & Wang, Y. (2022). Prediction of slag viscosity based on machine learning for molten gasification of hazardous wastes. Minerals, 12(12), 1525.

46. Li, M., Xu, J., Xiao, H., Liu, X., Yu, G., & Chen, X. (2023). Exploring influence of MgO/CaO on crystallization characteristics to understand fluidity of synthetic coal slags. Chinese Journal of Chemical Engineering, 53, 1–13.

47. Li, Y., Liu, X., Li, H., Cai, W., Lv, J., Duan, H., & Zhang, H. (2023). Research progress on high-temperature wetting behavior between slag and refractory. Journal of the Chinese Ceramic Society, 51(3), 677–686.

48. Liao, J., Qing, G., & Zhao, B. (2023). Phase equilibrium studies of the CaO-MgO-Al_2O_3-SiO_2 system for iron blast furnace slag: A review. Metals, 13(4), 801.

49. Lin, Y., Yu, Z., Liu, X., Yan, B., Fabritius, T., & Shu, Q. (2025). Viscosity and structure of low basicity CaO-SiO_2-10 wt.% FeO_x-10 wt.% P_2O_5 slag system. Journal of Non-Crystalline Solids, 668, 123796.

CC BY

JIRRS
Journal International Review of Research Studies

Received: 13/06/2026 - **Accepted:** 01/08/2026
Vol: 1.04
DOI: 10.66104/7x5etg23
Pages: 1-48

50. Liu, Q., Wang, W., Gao, M., Du, S., Yin, Y., & Zhang, J. (2025). Effect of CaO/SiO_2 and Al_2O_3/SiO_2 mass ratios on structure and viscosity of mold flux for continuous casting high-Mn high-Al steel. Steel Research International, 96, 2400740.

51. Liu, W., & Zuo, H. (2021). Effect of MnO and CaO substitution for BaO on the viscosity and structure of CaO-SiO_2-MgO-Al_2O_3-BaO-MnO slag. Journal of Non-Crystalline Solids, 567, 120940.

52. Liu, W., & Zuo, H. (2025). Influence of high-MnO on viscous properties of CaO-SiO_2-MgO-Al_2O_3-BaO-MnO slag. Steel Research International, 96, 2400806.

53. Liu, W., Chen, J., Pang, Z., Wang, J., Zuo, H., & Xue, Q. (2022). Investigation on the structure and viscosity of BaO-bearing slag melt through molecular dynamics simulation, Raman and 27Al MAS NMR spectra. Journal of Molecular Liquids, 359, 119342.

54. Liu, W., Pang, Z., Zheng, J., & Zuo, H. (2025). Properties evaluation of DRI smelting slag for molten iron production: Viscosity and sulfide capacity dependence on binary basicity. Journal of Iron and Steel Research International, 32(11), 4095–4107.

55. Liu, W., Pang, Z., Zheng, J., Yin, S., & Zuo, H. (2024). The viscosity, crystallization behavior and glass-ceramics preparation of blast furnace slag: A review. Ceramics International, 50, 18090–18104.

56. Liu, W., Qin, J., Zuo, H., Wang, J., & Xue, Q. (2024). Viscosity variations in the transition process of blast furnace slag towards high-Al_2O_3 and low-MgO content. Journal of Non-Crystalline Solids, 637, 123061.

57. Liu, Y., Wang, Q., Li, G., Zhang, J., Yan, W., & Huang, A. (2020). Role of graphite on the corrosion resistance improvement of MgO–C bricks to MnO-rich slag. Ceramics International, 46, 7517–7522.

58. Liu, Z., Cheng, K., Qiu, W., Zhang, R., Pan, S., Gao, Y., Wen, T., Zhang, L., Yuan, L., & Yu, J. (2025). Comprehensive review of the corrosion behavior of magnesia-based refractories by molten steel slag. Journal of Industrial and Engineering Chemistry, 145, 123–143.

CC BY

JIRRS
Journal International Review of Research Studies

Received: 13/06/2026 - **Accepted:** 01/08/2026
Vol: 1.04
DOI: 10.66104/7x5etg23
Pages: 1-48

59. Liu, Z., Wang, Y., & Xu, L. (2026). Composition design and property investigation of mold fluxes for the continuous casting of rare-earth weathering steel. Materials, 19(11), 2236.

60. Lyu, S., Ma, X., Chen, M., Huang, Z., Yao, Z., Wang, G., & Zhao, B. (2020). Application of phase equilibrium studies of CaO-SiO_2-Al_2O_3-MgO system for oxide inclusions in Si-deoxidized steels. Calphad, 68, 101721.

61. Lyu, Z., Jin, J., Gu, C., Wei, Z., Lyu, Z., Liu, Y., Li, H., Wang, B., & Bao, Y. (2025). Revealing the effect of FeO content on the structure and transfer properties of CaO–MgO–Al_2O_3–SiO_2–FeO slag systems: A molecular dynamic study. Journal of Molecular Liquids, 437(B), 128449.

62. Ma, W., Wang, C., Xu, J., & Yin, R. (2025). Influence of the MgO content and the CaO/Al_2O_3 ratio on the structure and transport properties of molten CaO–Al_2O_3–MgO slag systems: A molecular dynamics study. Metallurgical and Materials Transactions B, 56(5), 5821–5834.

63. Ma, W., Zhou, Y., Wei, C., Sheng, M., & Xu, J. (2026). Molecular dynamics insight into the oxygen network structure and its impact on transport characteristics of molten calcium aluminate electrolyte: The effect of FeO and SiO_2. Chemical Engineering Science, 333, 124247.

64. Madej, P. (2025). Influence of the reduction rate of slag from oxidation process of Cu–Fe–Pb alloy during reduction (de-coppering) on its viscosity. Metallurgical and Materials Transactions B, 56(1), 833–851.

65. Martin-Treceño, S., Allanore, A., Bishop, C. M., Marshall, A. T., & Watson, M. J. (2021). Implications of direct use of slag from ironmaking processes as molten oxide electrolyte. JOM, 73(6), 1899–1908.

66. Martin-Treceño, S., Allanore, A., Bishop, C. M., Watson, M. J., & Marshall, A. T. (2022). Determination of the partial contributions to the electrical conductivity of TiO_2–SiO_2–

CC BY

JIRRS
Journal International Review of Research Studies

Received: 13/06/2026 - **Accepted:** 01/08/2026
Vol: 1.04
DOI: 10.66104/7x5etg23
Pages: 1-48

Al_2O_3–MgO–CaO slags: Role of the experimental processing conditions. Metallurgical and Materials Transactions B, 53, 798–806.

67. Martin-Treceño, S., Weaver, J. S., Allanore, A., Bishop, C. M., Marshall, A. T., & Watson, M. J. (2020). Electrochemical behaviour of titanium-bearing slag relevant for molten oxide electrolysis. Electrochimica Acta, 354, 136619.

68. Meratian, M., Asgarian, A., Vadillo, A., Mostaghel, S., & Barati, M. (2021). A mathematical model for air atomization of molten slag based on integral conservation equations. Metallurgical and Materials Transactions B, 52, 4197–4205.

69. Mills, K. C., & Sridhar, S. (1999). Viscosities of ironmaking and steelmaking slags. Ironmaking & Steelmaking, 26(4), 262–268. https://doi.org/10.1179/030192399677121

70. Mo, R., Zhang, X., & Ren, Y. (2023). Influence of substituting B_2O_3 with Li_2O on viscosity, structure and crystalline phase of low-reactivity mold flux. International Journal of Minerals, Metallurgy and Materials, 30(7), 1320–1328.

71. Moliné, M. N., Galliano, P. G., & Tomba Martinez, A. G. (2026). How much does adhered ladle slag protect MgO-C refractories from oxidation? Next Materials, 10, 101473.

72. Muire, H., Zaaiman, S., & Zietsman, J. H. (2024). Slag physical property models and data: A review of structure, viscosity, electrical conductivity, and thermal conductivity. In Southern African Pyrometallurgy 2024 (pp. 189–205). Southern African Institute of Mining and Metallurgy.

73. Nagata, K., & Sasabe, M. (2020). Permeability coefficient of oxygen in molten slags and its mechanisms. ISIJ International, 60, 1872–1877.

74. Nazim, M. A., Emdadi, A., Sander, T., & O'Malley, R. (2025). The effect of mold flux wetting conditions with varying crucible materials on crystallization. Materials, 18(5), 1174.

75. Nigam, A., Lin, Y., Shu, Q., Biswas, K., & Sarkar, R. (2026). Viscosities of CaO–Al_2O_3 based non-reactive mold fluxes and their relationship to the structure of these slags. Journal of Non-Crystalline Solids, 687, 124152.

CC BY

JIRRS
Journal International Review of Research Studies

Received: 13/06/2026 - **Accepted:** 01/08/2026
Vol: 1.04
DOI: 10.66104/7x5etg23
Pages: 1-48

76. Pankka, I., Mulenshi, J., Taskinen, P., & Lindberg, D. (2026). Refractory wear in end-of-life Peirce–Smith converter bricks. JOM. Advance online publication.

77. Peng, L., Jiang, Z., & Geng, X. (2020). Design of ESR slag for remelting 9CrMoCoB steel through experiments and thermodynamic calculations. Calphad, 70, 101782.

78. Peng, Y., Li, S., Huang, A., & Gu, H. (2023). Effect of slag basicity on Turing pattern corrosion of alumina refractory ceramics in the presence of free radicals. Journal of the American Ceramic Society, 106(10), 6211–6220.

79. Pereira, A. C. (2026a). Ca–Al metallothermic reduction: A critical review of reductant design, reaction pathways, slag engineering, and scale-up. Journal International Review of Research Studies, 1(9), 1–49. https://doi.org/10.66104/bn5j2634

80. Pereira, A. C. (2026b). From Ti-bearing feed to aluminous slag: A critical review of sequential recovery and valorization pathways in aluminothermic titanium processing. International Journal of Research and Innovation in Social Science, 10(8), 5831–5864. https://doi.org/10.47772/IJRISS.2026.100800381

81. Pereira, A. C. (2026c). From upgraded titanium slag to modern metallurgical slag engineering: Technologies, industrial applications, and readiness—A critical review. International Journal of Current Science Research and Review, 9(8), 4556–4584. https://doi.org/10.5281/zenodo.22023255

82. Pereira, A. C. (2026d). Liquid-metal droplet coalescence in metallurgical slags: A critical review of interfacial phenomena, slag properties, hydrodynamics, kinetics, and metal recovery. International Journal of Research and Scientific Innovation, 10(7), 15007–15036. https://doi.org/10.47772/IJRISS.2026.100701023

83. Pereira, A. C. (2026e). Secondary aluminum dross and salt slag treatment: A critical review of integrated value recovery, risk control, and industrial readiness. International Journal of Current Science Research and Review, 9(8), 4428–4462. https://doi.org/10.5281/zenodo.21898845

CC BY

JIRRS
Journal International Review of Research Studies

Received: 13/06/2026 - **Accepted:** 01/08/2026
Vol: 1.04
DOI: 10.66104/7x5etg23
Pages: 1-48

84. Pereira, A. L., Morales Pereira, J. A., Bielefeldt, W. V., & Vilela, A. C. F. (2023). Thermodynamic evaluation of viscosity behavior for CaO-SiO_2-Al_2O_3-MgO slag systems examined at the temperatures range from 1500 to 1700 °C. Scientific Reports, 13, 16274.

85. Piao, Z., Zeng, K., Wang, Y., Zhang, C., Gao, M., & Liu, Y. (2023). Viscosity and structure of CaO–Al_2O_3–TiO_2-based mold fluxes with various CaO/Al_2O_3 mass ratios. Ironmaking & Steelmaking, 50(7), 828–836.

86. Qi, J., Wang, J., & Liu, C. (2026). Viscosity of low-reactive mold flux and its correlation with microstructure and crystalline phases. Crystals, 16(6), 375.

87. Qin, J., Liu, W., Wu, H., Wang, J., Xue, Q., Zhao, H., & Zuo, H. (2022). A comprehensive investigation on the viscosity and structure of CaO–SiO_2–Al_2O_3–MgO–BaO slag with different Al_2O_3/SiO_2 ratios. Journal of Molecular Liquids, 365, 120060.

88. Ren, H., Min, X., Ke, Y., Wang, Y., Peng, C., Li, Y., & Zhang, C. (2024). Mechanism study of lime decomposing fayalite melt: Thermodynamic basis for the sustainable and efficient recovery of iron resources from copper slag. Journal of Cleaner Production, 462, 142678.

89. Ribeiro, E. M., Cunha, M. V. R. da, Bicalho, N. C., Bueno, R. F. D., Costa, H. J., Duarte, A. K., Ribeiro, V. S., Silva, D. G. da, & Vasconcelos, W. L. (2026). Study of the wear of MgO-C refractory in the slag line of steel ladles. Tecnologia em Metalurgia, Materiais e Mineração, 23, e3353.

90. Riboud, P. V., Roux, Y., Lucas, L. D., & Gaye, H. (1981). Improvement of continuous casting powders. Fachberichte Hüttenpraxis Metallweiterverarbeitung, 19, 859–869.

91. Saigo, H., KC, D. B., & Saito, N. (2022). Einstein–Roscoe regression for the slag viscosity prediction problem in steelmaking. Scientific Reports, 12, 6541.

92. Saito, K., Morita, K., & Hasegawa, M. (2025). Criteria for thermodynamic properties of transition metal oxides in molten slags. Metallurgical and Materials Transactions B, 56, 5791–5799.

CC BY

JIRRS
Journal International Review of Research Studies

Received: 13/06/2026 - **Accepted:** 01/08/2026
Vol: 1.04
DOI: 10.66104/7x5etg23
Pages: 1-48

93. Sajid, M., Bai, C., Yu, W., You, Z., Tan, M., & Aamir, M. (2020). First principle study of electronic structural and physical properties of CaO-SiO_2-Al_2O_3 ternary slag system by using ab initio molecular and lattice dynamics. Journal of Non-Crystalline Solids, 550, 120384.

94. Sarkar, R., & Li, Z. (2021). Isothermal and non-isothermal crystallization kinetics of mold fluxes used in continuous casting of steel: A review. Metallurgical and Materials Transactions B, 52, 1357–1378.

95. Sharpless, L., Moon, J., & Chidambaram, D. (2024). Optical basicity: A review. Journal of Molecular Liquids, 394, 123803.

96. Shen, F., Zhang, G., Tian, J., Zheng, H., Gao, Q., & Jiang, X. (2024). Effect of TiO_2 on the structural properties and viscosity of CaO-SiO_2-8.25%MgO-15%Al_2O_3-TiO_2 slags. Journal of Non-Crystalline Solids, 640, 123114.

97. Shevchenko, M., & Jak, E. (2020). Thermodynamic optimization of the binary PbO–CaO and ternary PbO–CaO–SiO_2 systems. CALPHAD: Computer Coupling of Phase Diagrams and Thermochemistry, 70, 101807.

98. Shevchenko, M., & Jak, E. (2020). Thermodynamic optimization of the binary PbO–Cu_2O, Cu_2O–SiO_2 and ternary PbO–Cu_2O–SiO_2 systems. CALPHAD: Computer Coupling of Phase Diagrams and Thermochemistry, 69, 101774.

99. Shevchenko, M., & Jak, E. (2020). Thermodynamic optimization of the ZnO–FeO–Fe_2O_3–SiO_2 system. CALPHAD: Computer Coupling of Phase Diagrams and Thermochemistry, 68, 101735.

100. Shi, E.-Z., Tang, J., Chu, M.-S., & Tian, H.-Y. (2026). Structure-dependent electrical transport in CaO–MgO–FeO–SiO_2–Al_2O_3 oxide melts. Journal of Non-Crystalline Solids, 689, 124185.

101. Shi, E.-Z., Tang, J., Chu, M.-S., & Tian, H.-Y. (2026). Viscosity prediction and optimization of CaO-SiO_2-MgO-Al_2O_3 slag system based on integrated calibration of multi-source data. Journal of Iron and Steel Research International, 33(6).

CC BY

JIRRS
Journal International Review of Research Studies

Received: 13/06/2026 - **Accepted:** 01/08/2026
Vol: 1.04
DOI: 10.66104/7x5etg23
Pages: 1-48

102. Shishin, D., Hidayat, T., Fallah-Mehrjardi, A., Hayes, P. C., Decterov, S. A., & Jak, E. (2019). Integrated experimental and thermodynamic modeling study of the effects of Al_2O_3, CaO, and MgO on slag–matte equilibria in the Cu–Fe–O–S–Si–(Al, Ca, Mg) system. Journal of Phase Equilibria and Diffusion, 40(4), 445–461.

103. Shishin, D., Jak, E., & Decterov, S. A. (2018). Thermodynamic assessment of slag–matte–metal equilibria in the Cu–Fe–O–S–Si system. Journal of Phase Equilibria and Diffusion, 39(5), 456–475.

104. Shishin, D., Shevchenko, M., & Jak, E. (2021). Experimental study and thermodynamic calculations in the CaO–Cu_2O–FeO–Fe_2O_3–SiO_2 system for applications in novel copper-based processes. Journal of Sustainable Metallurgy, 7, 300–313.

105. Singh, M. K., Singh, K. K., & Pal, S. (2026). Predicting viscosity for steelmaking slag: A stacking regression approach. Ironmaking & Steelmaking, 53(1), 83–99.

106. Song, J., Liu, Y., Lv, X., & You, Z. (2020). Corrosion behavior of Al_2O_3 substrate by SiO_2–MgO–FeO–CaO–Al_2O_3 slag. Journal of Materials Research and Technology, 9(1), 314–321.

107. Song, Y., Hu, X., & Chou, K. (2023). Effect of Al_2O_3 on viscosity and structure of CaO-SiO_2-FeO_t-(Al_2O_3)-BaO slag. Ironmaking & Steelmaking, 50(11), 1521–1527.

108. Song, Y., Sun, Q., Zhang, H., Zhang, D., & Lv, Y. (2024). Effect of substituting CaO with BaO on viscosity and structure of CaO-SiO_2-FeO_t-Al_2O_3-BaO steel slag. Steel Research International, 95, 2400410.

109. Stepanenko, D. O., & Togobitska, D. M. (2026). Experimental investigation of viscosity and electrical conductivity of CaO-SiO_2-Al_2O_3-MgO blast furnace slags as structure-sensitive properties. Theory and Practice of Metallurgy, 2, 27–32.

110. Stovpchenko, G., Togobitskaya, D., Lisova, L., Stepanenko, D., & Medovar, L. (2022). Predictive models for molten slags viscosity and electrical conductivity based on directed chemical bonds concept. Ironmaking & Steelmaking, 49(6), 572–580.

CC BY

JIRRS
Journal International Review of Research Studies

Received: 13/06/2026 - **Accepted:** 01/08/2026
Vol: 1.04
DOI: 10.66104/7x5etg23
Pages: 1-48

111. Svantesson, J. L., Glaser, B., Ersson, M., White, J. F., Imris, M., & Jönsson, P. G. (2021). Study of dynamic refractory wear by slags containing very high FeO contents under steelmaking conditions. Ironmaking & Steelmaking, 48(5), 607–618.

112. Tan, J., Liu, Y., Wen, S., Deng, T., Chen, W., Li, N., Du, Y., & Kaptay, G. (2023). Modeling viscosity of SiO_2-Al_2O_3-CaO based slags using Arrhenius and VFT models as well as the CALPHAD method. Journal of Molecular Liquids, 385, 122259.

113. Taskinen, P. (2011). Direct-to-blister smelting of copper concentrates: The slag fluxing chemistry. Mineral Processing and Extractive Metallurgy, 120, 240–246.

114. Tian, Z., Kang, J., Yang, L., Wang, J., & Qiu, G. (2025). Effect of basicity on the viscosity and phase structure of chromium-containing high-titanium blast furnace slag. ISIJ International, 65(3), 333–340.

115. Urbain, G. (1987). Viscosity estimation of slags. Steel Research, 58(3), 111–116. https://doi.org/10.1002/srin.198701513

116. Vítková, M., Ettler, V., Johan, Z., Kříbek, B., Šebek, O., & Mihaljevič, M. (2010). Primary and secondary phases in copper-cobalt smelting slags from the Copperbelt Province, Zambia. Mineralogical Magazine, 74, 581–600.

117. Wang, C., Xie, C., Xu, J., & Wan, K. (2025). Wettability and spreading kinetics between some refractory materials and molten calcium aluminate slag. Steel Research International, 96(9), 156–175.

118. Wang, H., Zhao, R., Jia, Z., Yang, Y., & Sun, H. (2026). Erosion resistance evaluation of ceramic crucible in oxide-fluoride slags: Application to high-temperature molten oxide electrolysis. Ceramics International, 52(13B), 23087–23095.

119. Wang, Q.-M., Huang, M.-X., Yan, S.-Y., Wang, S.-S., Tian, Q.-H., & Guo, X.-Y. (2023). Hydrodynamic simulation of metal droplet settlement in molten slag. Transactions of Nonferrous Metals Society of China, 33(4), 1244–1257.

CC BY

JIRRS
Journal International Review of Research Studies

Received: 13/06/2026 - **Accepted:** 01/08/2026
Vol: 1.04
DOI: 10.66104/7x5etg23
Pages: 1-48

120. Wang, W., Xu, H., Zhai, B., & Zhang, L. (2022). A review of the melt structure and crystallization behavior of non-reactive mold flux for the casting of advanced high-strength steels. Steel Research International, 93, 2100073.

121. Wei, J., Han, B., Ma, L., Xiang, X., Zhang, Y., Dong, B., Wan, Z., Yan, J., Zhu, Y., Chen, J., & Ma, J. (2025). Corrosion behavior of MgO-C refractories with Al_2O_3-spinel addition by different low basicity slags. Ceramics International, 51(14), 18439–18450.

122. Weiss, J. P., Munchen, D. D., Lucas, H., & Friedrich, B. (2026). Fayalitic minerals and slags (Part I): A survey on composition and potential for phases design. Journal of Sustainable Metallurgy, 12, 2365–2384.

123. Wiencke, J., Lavelaine, H., Panteix, P.-J., Petitjean, C., & Rapin, C. (2020). The impact of iron oxide concentration on the performance of molten oxide electrolytes for the production of liquid iron metal. Metallurgical and Materials Transactions B, 51, 365–376.

124. Wu, X., Hu, X., Xu, J., Su, L., & Zhang, J. (2022). Wetting and interfacial tension of molten $CaO–Al_2O_3–MgO–FeO$ slag and BN substrate. Journal of Materials Research and Technology, 16, 764–772.

125. Xia, B., Jiao, F., Li, H., Hu, Y., Liu, J., Zhang, Y., Liu, T., & Mao, M. (2024). Relation between the viscosity and electrical conductivity of molten slag for coal gasification and their dependence on SiO_2 content. Chemical Engineering Research and Design, 207, 142–150.

126. Xiao, W., Yao, S., Zhou, S., & Wang, H. (2022). Evolution of the structure and viscosity of copper slag during metallization-reduction. Journal of Alloys and Compounds, 903, 163751.

127. Xie, C., Yin, R., Xu, J., Hu, X., Wu, X., & Zhang, J. (2025). Wettability of molten $CaO–Al_2O_3–MgO$ slag on some refractory materials at 1773 K. Ironmaking & Steelmaking, 52(4–5), 464–476.

CC BY

JIRRS
Journal International Review of Research Studies

Received: 13/06/2026 - **Accepted:** 01/08/2026
Vol: 1.04
DOI: 10.66104/7x5etg23
Pages: 1-48

128. Xie, S., Wang, Q.-M., Guo, X.-Y., Liao, C.-F., & Zhao, B.-J. (2025). Phase equilibria of slag systems “FeO”-SiO_2-CaO-Al_2O_3 and “FeO”-SiO_2-CaO-MgO at 1200 °C and p(O2) of 10−7 kPa. Transactions of Nonferrous Metals Society of China, 35(1), 338–348.

129. Xing, X., Pang, Z., Mo, C., Wang, S., & Ju, J. (2020). Effect of MgO and BaO on viscosity and structure of blast furnace slag. Journal of Non-Crystalline Solids, 530, 119801.

130. Xuan, W., Zhao, C., Ma, Z., Liu, Z., & Zhang, J. (2025). Data-driven machine learning methods to predict the viscosity-temperature characteristics for gasification slags. Fuel, 398, 135287.

131. Yan, W., Shen, Y., Chen, S., & Wang, Y. (2024). Viscosity and melting temperature prediction of mold fluxes based on explainable machine learning and SHapley additive exPlanations. Journal of Non-Crystalline Solids, 636, 123037.

132. Yan, X., Wang, W., Zhou, L., Yang, Y., Lin, H., & Liu, X. (2024). Effect of MgO on viscosity and melt structure of mold flux for continuous casting. Ironmaking & Steelmaking, 51(3), 262–270.

133. Yang, B., Hou, J., Chen, J., Bai, C., Zhang, S., & Hu, M. (2025). Study of fluidity and structure of blast furnace slag controlled by TiO_2 and Al_2O_3 coupling. Ironmaking & Steelmaking. Advance online publication.

134. Yang, J., Chen, D., Long, M., & Duan, H. (2020). An approach for modelling slag infiltration and heat transfer in continuous casting mold for high Mn-high Al steel. Metals, 10(1), 51.

135. Yang, Y., Wang, W., Zhou, L., Zhong, X., Zheng, Q., & Zhao, R. (2023). Melting and crystallization behaviors of mold flux with the addition of waste electrolyte. Steel Research International, 94, 2300211.

136. Yao, Z., Ma, X., & Lyu, S. (2021). Phase equilibria of the Al_2O_3-CaO-SiO_2-(0%, 5%, 10%) MgO slag system for non-metallic inclusions control. Calphad, 72, 102227.

CC BY

JIRRS
Journal International Review of Research Studies

Received: 13/06/2026 - **Accepted:** 01/08/2026
Vol: 1.04
DOI: 10.66104/7x5etg23
Pages: 1-48

137. Yeo, T.-M., Cho, J.-W., Alloni, M., Casagrande, S., & Carli, R. (2020). Structure and its effect on viscosity of fluorine-free mold flux: Substituting CaF_2 with B_2O_3 and Na_2O. Journal of Non-Crystalline Solids, 529, 119756.

138. Yin, R., Xie, C., Xu, J., Sheng, M., & Guo, H. (2026). Wettability and spreading kinetics of $CaO–Al_2O_3–MgO$ molten slag on Al_2O_3 substrate with applied voltage. Metallurgical and Materials Transactions B, 57(5), 2906–2922.

139. Yu, Y., Liu, W., & Zuo, H. (2023). Viscosity and desulphurisation behaviour of $CaO-SiO_2-MgO-Al_2O_3-BaO-MnO$ slag. Ironmaking & Steelmaking, 50(10), 1420–1426.

140. Yu, Z.-B., Xu, S.-Y., An, L.-Z., Zang, X.-M., Chen, Y.-X., Li, S.-S., Yang, J., & Kong, L.-Z. (2026). Viscosity and electrical conductivity of $CaF_2-CaO-Al_2O_3-MgO-Ce_2O_3$ electroslag remelting slag. Ironmaking & Steelmaking, 53(4), 736–745.

141. Yuan, Z., & Zhu, L. (2022). Effect of Li_2O on rheological properties, structure, and crystallization of mold flux for high-speed thin-slab continuous casting. Ironmaking & Steelmaking, 49(2), 226–237.

142. Zaaiman, S., Muire, H., & Zietsman, J. H. (2024). Slag physical property determination: An overview of experimental and computational methods to determine structure, viscosity, electrical conductivity, and thermal conductivity. In Southern African Pyrometallurgy 2024. Southern African Institute of Mining and Metallurgy.

143. Zhang, L., You, J., Liu, G., Xia, X., Zhao, Y., Xu, F., Sheng, M., Lu, J., Liu, Y., Zhang, Q., Wan, S., Lu, L., & Tang, K. (2026). Decoding viscosity-microstructure relationships in the ternary $CaO-SiO_2-Fe_xO$ system via integrated machine learning and multimodal characterization. Journal of Materials Science & Technology, 250, 299–308.

144. Zhang, L., Yue, Q., & Yang, H. (2021). Kinetics and mechanism of non-isothermal oxidation for $FeO–SiO_2–CaO$ ternary copper slag system. Reaction Kinetics, Mechanisms and Catalysis, 134, 903–916.

CC BY

JIRRS
Journal International Review of Research Studies

Received: 13/06/2026 - **Accepted:** 01/08/2026
Vol: 1.04
DOI: 10.66104/7x5etg23
Pages: 1-48

145. Zhang, R., Min, Y., & Wang, Y. (2020). Viscosity estimation of multicomponent slags of the $CaO–SiO_2–Al_2O_3–Fe_xO$ system based on microstructure analysis. Energy & Fuels, 34(7), 8129–8138.

146. Zhang, S., Zhang, J., Wang, Z., Jiang, D., Liang, Z., & Zhang, S. (2025). Effect of basicity on the structure and viscosity properties of HIsmelt slag: A molecular dynamics simulation. Canadian Metallurgical Quarterly, 64(3), 799–807.

147. Zhang, W., He, F., & Xiao, Y. (2020). Structure, viscosity, and crystallization of glass melt from molten blast furnace slag. International Journal of Applied Glass Science, 11(4), 676–684.

148. Zhang, Y.-H., Zhu, T.-B., Guo, W.-J., Zhao, X., Li, Y.-W., Liao, N., Wang, H., Sang, S.-B., & Yan, W. (2026). A review of slag corrosion resistance of MgO-C refractories: Methods, mechanisms and improvements. Journal of Iron and Steel Research International, 33(2), 66.

149. Zhao, A., Tan, M., Liu, W., Zhu, G., Gu, S., Li, T., & Zhang, F. (2024). An in-situ investigation on the microstructure and viscosity characteristic of mold flux during slag-metal reaction process. Computational and Theoretical Chemistry, 1237, 114653.

150. Zhao, B., Hayes, P., & Jak, E. (2013). Effects of CaO, Al_2O_3, and MgO on liquidus temperatures of copper smelting and converting slags under controlled oxygen partial pressures. Journal of Mining and Metallurgy, Section B: Metallurgy, 49(2), 153–159.

151. Zhao, J., Qu, B., & Cui, Y. (2021). Viscosity estimation model of fluorine-containing mold flux for continuous casting. PLOS ONE, 16(3), e0247828.

152. Zhao, Q., Zheng, X., Liu, C., Jiang, M., Saxén, H., & Zevenhoven, R. (2021). Corrosion behavior of MgO-C ladle refractory by molten slag. Steel Research International, 92, 2000497.

153. Zheng, D.-L., Ma, G.-J., Zhang, X., Liu, M.-K., & Xu, J. (2023). Effect of CaO/Al_2O_3 on structure, viscosity, and surface tension of electroslag remelting-type CeO_2-bearing slag. Journal of Iron and Steel Research International, 30(4), 717–725.

CC BY

JIRRS
Journal International Review of Research Studies

Received: 13/06/2026 - **Accepted:** 01/08/2026
Vol: 1.04
DOI: 10.66104/7x5etg23
Pages: 1-48

154. Zhou, W., Li, T., Lan, D., Sun, C., & Yang, S. (2023). Influence of TiO_2, Al_2O_3, and basicity on viscosity and structure of high titanium-bearing blast furnace slag. Materials, 16(7), 2575.

155. Zou, Y., Huang, A., & Gu, H. (2020). Novel phenomenon of quasi-volcanic corrosion on the alumina refractory–slag–air interface. Journal of the American Ceramic Society, 103(11), 6639–6649.

CC BY